NASA/TM—1999–209009

A TREETOPS Simulation of the STABLE Microgravity Vibration Isolation System

G.S. Nurre and M.S. Whorton
Marshall Space Flight Center, Marshall Space Flight Center, Alabama

Y.K. Kim
University of Alabama in Huntsville, Huntsville, Alabama

National Aeronautics and
Space Administration

Marshall Space Flight Center

January 1999

Available from:

NASA Center for AeroSpace Information
800 Elkridge Landing Road
Linthicum Heights, MD 21090–2934
(301) 621–0390

National Technical Information Service
5285 Port Royal Road
Springfield, VA 22161
(703) 487–4650

TABLE OF CONTENTS

I. INTRODUCTION 1

II. STABLE SYSTEM DESCRIPTION 4

A. STABLE Hardware 4
B. STABLE Control Algorithms 5

III. DESCRIPTION OF STABLE TREETOPS MODEL 9

A. STABLE Structural Model 10
B. STABLE Sensors Model 12
C. STABLE Actuator Model 13
D. STABLE Controller Implementation 14

IV. SIMULATION RESULTS 16

A. Case 1: Transient Response Analysis With Initial Displacement 17
B. Case 2: Transient Response Analysis With Initial Excitation 27
C. Case 3: Attenuation Performance Analysis Results 27

V. CONCLUSIONS 37

APPENDIX A—Derivation of Relative Position at the Actuator Gap 38

A.1 Center of Mass Relative Displacements 38
A.2 Relative Displacements at the Actuator Gap 43

REFERENCES 46

LIST OF FIGURES

1. Microgravity acceleration requirements 1
2. Configuration of STABLE system 4
3. STABLE general block diagram 5
4. Position loop controller block diagram 7
5. Mode switch regions for position controller 7
6. STABLE coordinate systems 9
7. PID position controller output with initial displacement 19
8. Detailed PID position controller output with initial displacement 20
9. Detailed PID position controller output with initial displacement (Continued) 21
10. Detailed PID position controller output of sixth channel with initial displacement 22
11. Output of accelerometers with initial displacement 23
12. Output of position sensors with initial displacement 24
13. Position error at the CM of STABLE platform with initial displacement 25
14. Position error at the center of actuators gap with initial displacement 26
15. PID position controller output with initial excitation 28
16. Detailed PID position controller output with initial excitation 29
17. Detailed PID position controller output with initial excitation (Continued) 30
18. Detailed PID controller output of sixth channel with initial excitation 31
19. Output of accelerometers with initial excitation 32
20. Output of position sensors with initial excitation 33

LIST OF FIGURES (Continued)

21. Position error at the CM of STABLE platform with initial excitation 34

22. Position error at the center of actuators gap with initial excitation 35

23. Acceleration attenuation curve of STABLE system 36

24. Definition of coordinate frames for relative position measurements 39

25. Position sensor detector locations 39

26. Error vector projection for sensor #1 41

27. Relative displacement vector at actuator gap 43

28. Actuator coordinate frames 44

LIST OF TABLES

1. Node definitions of TREETOPS STABLE body #1 11
2. Node definitions of TREETOPS STABLE body #2 11
3. Hinge definitions of STABLE TREETOPS model 11
4. Definition of TREETOPS STABLE sensors model 13
5. Definition of TREETOPS STABLE actuators model 14
6. Mass properties of the STABLE platform 16
7. STABLE control parameters 17
8. Acceleration biases of six accelerometers 17

TECHNICAL MEMORANDUM

A TREETOPS SIMULATION OF THE STABLE MICROGRAVITY VIBRATION ISOLATION SYSTEM

I. INTRODUCTION

As a research facility for microgravity (μg) science, the *International Space Station* (*ISS*) will be used for numerous investigations such as protein crystal growth, combustion, and fluid mechanics experiments which require a quiescent acceleration environment across a broad spectrum of frequencies. Examples of the acceleration requirements for these processes are shown in figure 1. Shown are the maximum magnitudes of acceptable accelerations, measured relative to nominal acceleration of gravity at the Earth's surface, versus frequency, and the expected acceleration environment in the experiment. Note that these experiments are most sensitive to low frequency accelerations and can tolerate much higher accelerations at higher frequency. However, the anticipated acceleration environment on the *ISS* significantly exceeds the requirements shown in figure 1. The ubiquity of vibratory acceleration disturbance sources and the difficulty in characterization of these sources precludes source isolation, requiring vibration isolation to attenuate the anticipated disturbances to an acceptable level in the experiment.

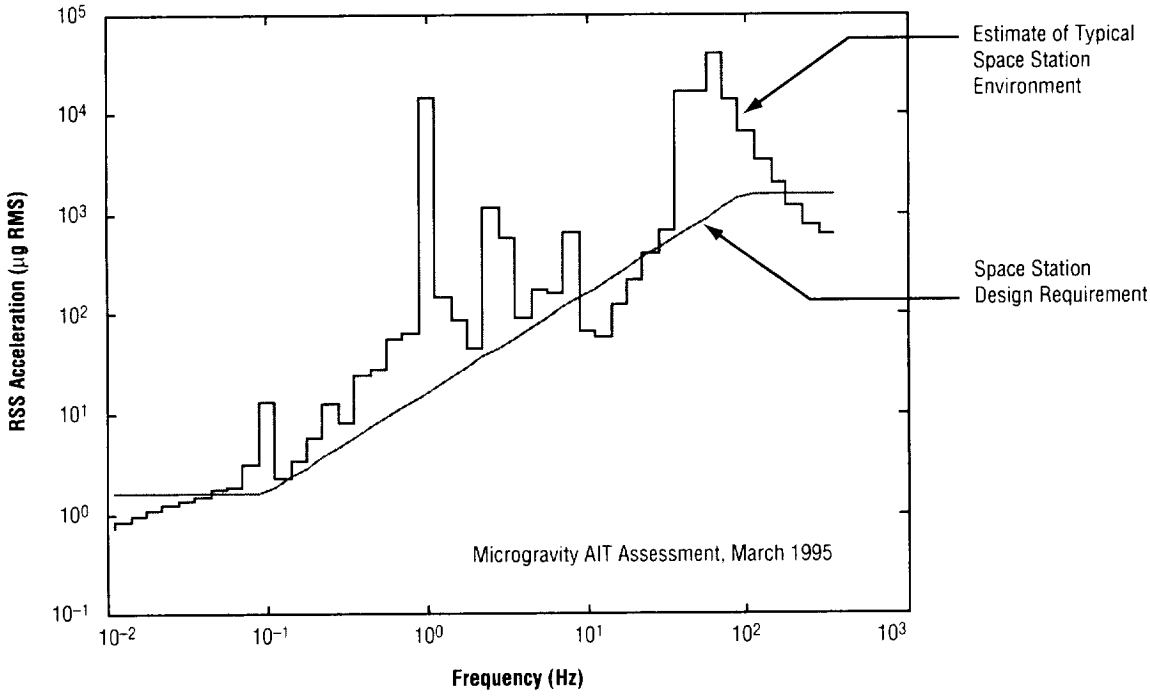

Figure 1. Microgravity acceleration requirements.

The primary sources of vibration on the *ISS* can be categorized into three characteristic frequency ranges. At low frequencies, ~10^{-3} Hz, the dominant accelerations are caused by gravity gradients and atmospheric drag. At high frequencies, above ~1 Hz, the vibrations are caused by sinusoidal steady-state sources such as pumps, compressors, electric motors, and fans, as well as transient sources such as impacts, astronaut motion, and high frequency components of thruster firings. The third characteristic frequency range of vibrations is the intermediate range of ~10^{-3} to 1 Hz. The sources of accelerations in this range are mostly transient in nature, such as the motion of astronauts and payloads around the *ISS*, as well as motion of the *ISS* caused by thrusters. Because of their transient nature, the effect of these vibrations on many experiments is difficult to analyze. The calculation of the resultant accelerations of the ISS are also complicated by the interaction of these vibration sources with the structural modes of the *ISS*, at least at the upper end of this frequency range. In the high frequency range, passive isolation techniques are often adequate to provide sufficient attenuation of vibration disturbances. However, isolation of low and intermediate frequency vibrations is not possible with passive isolation and requires active isolation. Hence, the development of active isolation systems is necessary to provide a quiescent acceleration environment as required by many microgravity science investigations.

The basic objective of a vibration isolation system is to constrain the acceleration environment in the experiment by attenuating accelerations transmitted from the base to the isolated platform via umbilicals or other direct disturbances. Base motion may be due to several sources such as crew motion, vehicle attitude control, or mechanical systems. In addition, disturbance forces which are transmitted directly to the platform (independent of the umbilicals) may result from crew contact or payload-generated sources such as pumps, fans, motors, and structural vibration of the isolated experiment. The required attenuation can be derived from the anticipated disturbance environment and required acceleration levels as shown in figure 1. To provide the desired environment requires that the isolation system pass through the quasi-steady accelerations while providing attenuation above 0.01 Hz. At frequencies above 10 Hz, the required attenuation level is –60 dB, or 3 orders of magnitude of attenuation. To accomplish this, isolation in the presence of realistic umbilicals while rejecting direct disturbances requires an active isolation system. By sensing relative position and absolute acceleration of the platform, the control system causes the platform to follow the very low frequency motion of the base while attenuating the base motion above 0.01 Hz. High bandwidth acceleration feedback effectively increases the payload mass for disturbance rejection. Demonstration of this level of performance in 6 degrees of freedom (DOF) using hardware cannot be accomplished on the ground due to gravitational coupling, but requires testing in a microgravity environment. Long periods of experimentation are necessary to characterize the low frequency behavior, which is the most critical frequency range for active vibration isolation.

For several years, an extensive effort has been underway in the aerospace community to develop active isolation systems for microgravity science experiments. A joint effort by the Marshall Space Flight Center (MSFC) and McDonnell Douglas Aerospace (MDA) culminated in the design and flight test of the Suppression of Transient Accelerations By Levitation (STABLE) system. STABLE was the first successful flight test of an active isolation device for microgravity science payloads and was flown

on STS–73/USML–2 in October 1995.[1] Aside from being the first active microgravity vibration isolation system to be successfully implemented in orbit, STABLE was also significant in its development process. In less than 5 months, STABLE was designed, fabricated, tested, qualified, and delivered to the Kennedy Space Center. Nor is it trivial that the process was jointly conducted by NASA/MSFC in Huntsville, AL, and MDA in Huntington Beach, CA. The accelerated schedule and distributed location of the design team made imperative the use of a high-fidelity simulation for analysis and design.

In order to verify the control system design and estimate on-orbit performance of STABLE, a high-fidelity, nonlinear, multibody simulation was developed using TREETOPS.[2] TREETOPS is a time history simulation developed for analysis of the dynamics and control-related issues of multibody structural systems. The name "TREETOPS" is indicative of the tree topology of linked multiple bodies, each of which may be rigid or flexible, with translations and large angle rotations between each body. Kane's method is employed in the derivation of the equations of motion, which are numerically integrated to generate the time history response of the system. Extensive control system modeling capabilities are incorporated in TREETOPS, including a host of sensors and actuators along with controller models in the form of block diagram (transfer function), state space (multi-input/multi-output), and user-defined continuous or discrete controllers. An interactive setup program allows a convenient, easy-to-use interface with the simulation for model definition, input data editing, and error checking. For more detailed information on the analytical formulation and modeling aspects of TREETOPS, the reader is referred to the user's guide.[2]

This report is written to document the development of the TREETOPS simulation of STABLE used in support of control system design. Because of the aggressive design, development, and delivery schedule for STABLE, sufficient time was not available for development of an accurate control design model. Instead, each of the six independent control channels were designed, based on a 1-DOF approximation, and then analyzed and refined using the high-fidelity STABLE TREETOPS model. Hence, the STABLE TREETOPS model was essential for the successful design and flight test of STABLE. Section II describes the STABLE flight hardware and control system and section III is a parallel description of the simulation implementation of STABLE. Simulation results and results of the performance analysis of the STABLE system using TREETOPS are presented in section IV with conclusions in section V.

II. STABLE SYSTEM DESCRIPTION

A. STABLE Hardware

STABLE is comprised of a middeck locker, an isolated platform on which a thermal fluid convection experiment is mounted, three actuator assemblies, nine acceleration sensors, three position sensors, and associated electronics and control boards. The major elements of STABLE are shown in figure 2 (taken from ref. 1). The platform is suspended from the base of the locker box by three electromagnetic actuators developed by MDA. The only physical connections between the isolated platform and the base are flexible umbilicals that provide power and data to and from the platform.

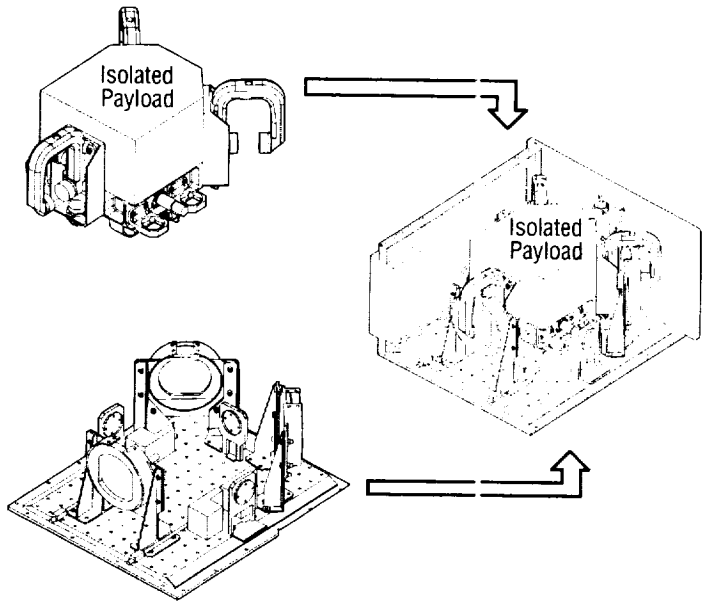

Figure 2. Configuration of STABLE system.

Each actuator assembly provides two axes of force with a gap that allows ±1 cm of travel in each axis. This "sway space" is required to provide isolation from the very low frequency motion of the vehicle. The actuator is comprised of a paddle-shaped armature mounted to the base of the locker and a horseshoe magnet composed of an iron horseshoe and two Samarium-Cobalt pole pieces that produce a concentrated magnetic field in the gap between the poles. The armature paddle is inserted between the two permanent magnets of the horseshoe bracket as illustrated in figure 2. The coil assembly contains two independent coils, oriented such that when a current is passed through them, two independent orthogonal forces are produced in the plane, normal to the field lines of the permanent magnet. By varying the current in the armature coils, a force is induced on the platform that is used to attenuate

disturbances and provide a quiescent acceleration environment on the platform. A high frequency acceleration feedback control loop and a low frequency position feedback control loop are implemented to produce the required control force. The control algorithms are described in the next section.

Six accelerometers and three relative position sensors are used to sense the isolated platform motion. The accelerometers are mounted in pairs on each of the three actuator mounting brackets and oriented to measure acceleration along the actuator force directions. Three additional accelerometers are mounted on the base and provide a measure of the base environment. The accelerometers used on both the platform and the base are model QA–2000, made by Sunstrand. Each of the three position sensors measures relative position of the platform with respect to the base at its particular location in two orthogonal axes. It is composed of a laser illuminator, mounted on the platform, that projects a laser image across the sway space onto a photoresistive detector fixed to the base. The position of the platform with respect to the base is determined by processing the signals from the detector which indicate the location of the laser image on the face of the detector.

B. STABLE Control Algorithms

The key to the robust performance of STABLE is its six independent position and acceleration loops which provide high bandwidth acceleration feedback along with a positioning system that is insensitive to drift. A block diagram of this system is shown in figure 3.

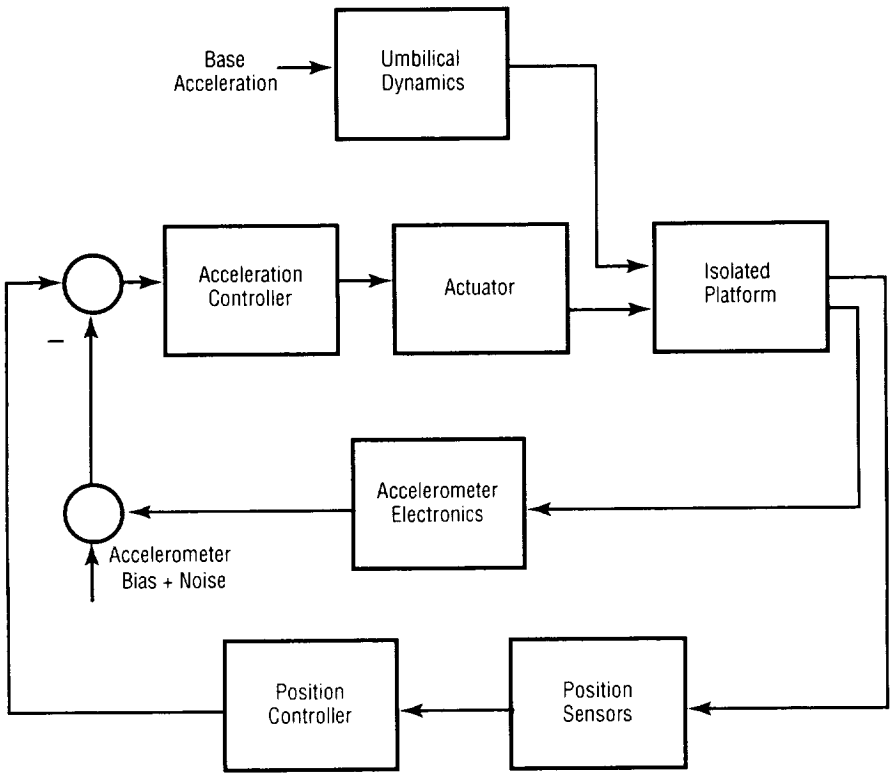

Figure 3. STABLE general block diagram.

The low bandwidth digital position controller uses measurements from the position sensors to compute the 6-DOF displacement of the floating platform and keep the floating platform centered in the sway space over a period of minutes. The acceleration loop is an analog controller with an ~50-Hz bandwidth to null the sensed acceleration of the platform.

1. Position Controller

A vibration isolator must attenuate "high-frequency" vibrations and be able to move with respect to the support structure and, thus, maintain an inertial position (or velocity) while the surrounding structure is in motion. To accomplish this, space must be provided around the isolated structure for it to "sway" back and forth. The geometry of the sway space determines the lower frequency limit for attenuation of base motion. Below this low frequency limit, quasi-steady forces must be transmitted to the platform so that the platform will follow the low frequency motion of the support structure. The position controller serves this purpose.

The position loop is a digital proportional-integral-derivative (PID) controller which uses sensor measurements to compute the position of the actuator with respect to a nominal centered position. Integral control is used to compensate for the error in calibration of accelerometer bias, unknown umbilical bias force, and accelerometer bias drift due to temperature variation. Since the position sensors are not coincident with the actuators, they do not provide a direct measure of displacement in the input axis of the actuator, and additional computations are performed in the digital processor to determine the position errors at the actuator gap. The algorithm for computing relative position at the gap from remote position sensor measurements is described in appendix A. Once computed, they are passed to the position controller, also in the digital processor, which calculates acceleration commands to each actuator. These acceleration commands are summed with the accelerometer signals and form the error signal input to the acceleration loop control law.

The position control law operates in either of two modes, depending on the calculated actuator gap. While the gap position error is small, low PID gains are used to provide a very small restoring force which will not violate the acceleration requirements. If the gap error becomes large (meaning the platform is nearing the boundaries of its sway space), a set of high gains effectively increases the spring constant of the control law to prevent the platform from making mechanical contact. A block diagram of the position control loop is given in figure 4.

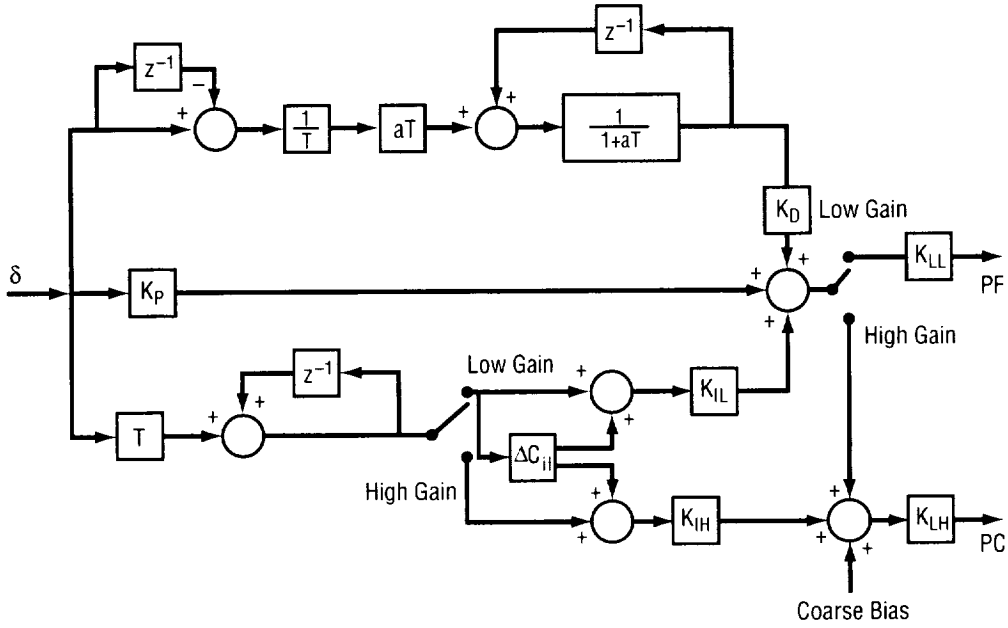

Figure 4. Position loop controller block diagram.

Figure 5 illustrates the logic employed for mode selection. Given the set of position error measurements, the high or low gain mode is determined by checking the magnitude of each error $\delta_i (i = 1,\cdots,6)$ for all six channels, as follows:

- If during the previous sample period the high gain mode was in effect and the magnitude of any δ_i is less than radius-low (RL), switch to low gain mode.
- If during the previous sample period the low gain mode was in effect and the magnitude of any δ_i is greater than radius-high (RH), switch to high gain mode.

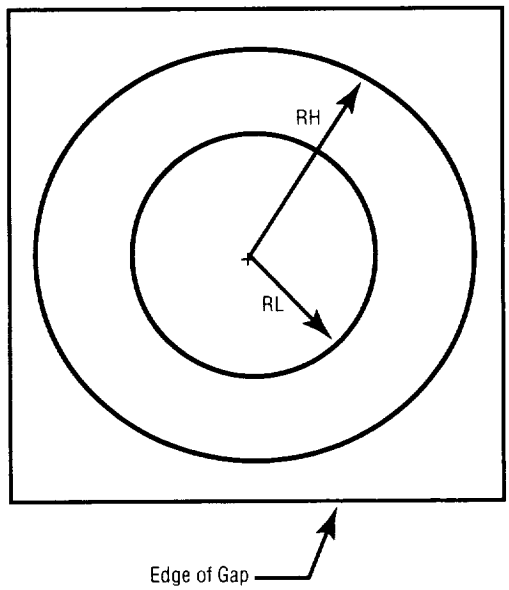

Figure 5. Mode switch regions for position controller.

The gap error signal is input to the position controller which is passed through proportional, derivative, and integral channels. Two digital-to-analog (D/A) converters with different resolutions are used for the output. Fine resolution output signals are sent through a 12-bit D/A converter with a resolution of 0.1 μg (200 μg full-scale) and coarse output signals use a larger range 12-bit D/A converter with a 10 μg resolution (20,000 μg full-scale). The derivative channel is low pass filtered to reduce high-frequency noise generated by differentiation. Logic is employed in the integral channel to reduce the excess that may be present due to buildup of large errors. While in low gain mode, the integral channel signal may become larger than can be adequately dealt with by the fine resolution output D/A converter, and thus the channel may be incrementally unloaded through the coarse channel D/A converter. The integral channel signal is compared with a maximum allowable value and if the signal is too large, an integer multiple of the coarse D/A converter least significant bit (10 μg) is subtracted from the fine channel and added to the coarse channel output. The integral channel for both fine and coarse outputs are checked for saturation prior to summing with other signals.

2. Acceleration Controller

The analog acceleration controller attempts to mitigate acceleration disturbances sensed by the accelerometers. The analog accelerometer measurement forms the acceleration error signal input to the analog acceleration controller. A rate feedback-type acceleration controller provides stability robustness since the actuator and sensor are spatially collocated. A low pass filter provides rolloff at a nominal bandwidth of 50 Hz. Performance of the acceleration loop is limited by controller bandwidth, accelerometer noise, resolution- and temperature-dependent bias variations, and disturbances transmitted through the umbilical connections. The output from the acceleration loop is the current command to the actuator coils. The acceleration control loop is implemented in TREETOPS with the transfer function

$$\text{Acceleration Control} = \frac{K_A(s+10*2\pi)}{10s(s+2\pi)} \text{ (N/m/s}^2\text{)} \ ,$$

where $K_A = 5.5 \times 10^4$.

The next section describes the TREETOPS implementation of the STABLE dynamics and control algorithms.

III. DESCRIPTION OF STABLE TREETOPS MODEL

In order to verify the control system and estimate the performance of STABLE in the orbital environment, a detailed structural and control model of STABLE was developed for TREETOPS. Since the platform of STABLE is floating freely within the STABLE locker box that is rigidly attached to the space shuttle, the STABLE system was modeled as two rigid bodies (first body for the space shuttle and rigidly attached locker box and second body for the isolated platform). The only physical connections between the platform and base are the umbilical cables (that transfer data and power between the platform and base) which are modeled as a 6-DOF hinge connection with spring stiffness specified to match the dynamic properties of the umbilical cables.

The TREETOPS model of the STABLE system must accurately model all of the actual flight hardware components to precisely represent the flight system. Note that TREETOPS terminology is indicated by spelling with capital letters. The STABLE actuator that yields two orthogonal forces can be modeled using two TREETOPS JET actuators and each STABLE accelerometer sensor can be modeled using the TREETOPS ACCELEROMETER sensor. Actuator and sensor models are idealized and do not include high-frequency dynamics. Since there is no built-in TREETOPS position sensor model that exactly corresponds to the STABLE position sensor, a mathematical position sensor model was developed using the built-in TREETOPS POSITION VECTOR sensor and STAR sensor. This position sensor model was implemented in a user-defined discrete controller subroutine and incorporated with the main TREETOPS dynamics simulation. The convention of the local coordinates and locations of the actuators and sensors are shown in figure 6. In this figure, F_{ij}, A_{ij}, and e_{ij} denote jth force component of ith actuator, jth acceleration component of ith accelerometer, and jth position error component of ith position sensor, respectively (1st, 2nd, and 3rd components stand for x, y, and z axis components, respectively).

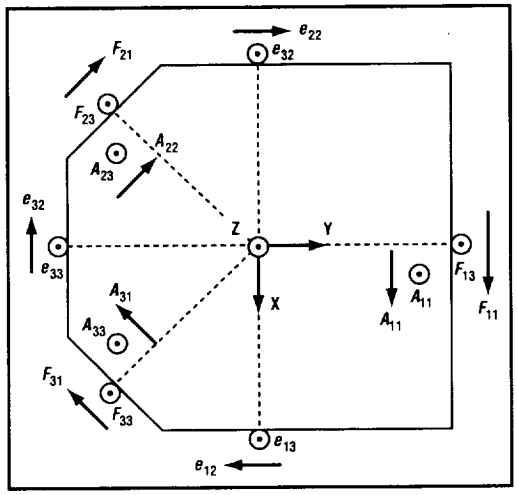

Figure 6. STABLE coordinate systems.

With supplied mass properties (mass and moments of inertia) of the two bodies and the locations of center of mass (CM), actuators, accelerometers, position sensors, and umbilical connections, TREETOPS determines the kinematics and dynamics of the STABLE system. The fast, continuous-acceleration control loop was implemented in the STABLE TREETOPS model using the built-in TREETOPS continuous block diagram controller and the slow digital position control loop was implemented in the STABLE TREETOPS model using a user-defined discrete controller subroutine.

A. STABLE Structural Model

The STABLE system, including the space shuttle, was modeled as two rigid bodies connected by linear and nonlinear quadratic springs. Since the objective of the STABLE controller is to achieve attenuation of an acceleration disturbance from the locker box to the STABLE platform, the space shuttle and attached locker box was modeled as one arbitrary rigid body that gives a disturbance to the STABLE platform through umbilical cables.

According to the TREETOPS tree topology, the space shuttle and attached locker box is defined by body #1 and linked by hinge #1 with 6 DOF (3 rotational and 3 translational) with respect to the origin of the inertial coordinate system. The platform floating inside the locker box is defined by body #2 and connected to body #1 through hinge #2 with 6 DOF. The umbilical connection between the platform and locker box is modeled as the combination of six linear spring devices and two quadratic spring devices with a 10-m undeformed length. This undeformed length was used to produce the desired linear force without introducing artificial rotational coupling.

For body #1, 12 nodal points are chosen to represent the CM, origin of local coordinate system of body #1, three position sensor detector attach points, the CM of body #2, and six umbilical cord attach points. For body #2, 16 nodal points are chosen to represent the CM, origin of local coordinate system of body #2, three actuator attach points, six accelerometer attach points, three position sensor laser attach points, and two umbilical cord attach points. Table 1 summarizes the nodes of body #1 (for example, B1N2 denotes node #2 of body #1) and the nodes of body #2 are summarized in table 2 (for example, B2N2 denotes node #2 of body #2). The definitions of all hinges of STABLE TREETOPS model are summarized in table 3.

Table 1. Node definitions of TREETOPS STABLE body #1.

Node	Description	Location in Body Coordinates (meter)
B1N1	CM of body #1	(0,0,0.02)
B1N2	Origin of body #1 coordinate	(0,0,0)
B1N3	Position sensor laser #1	(0.1537,0,0)
B1N4	Position sensor laser #2	(–0.1537,0,0)
B1N5	Position sensor laser #3	(0,–0.1537,0)
B1N6	CM of body #2	(0.004,–0.02,0.067)
B1N7	*X* umbilical #1	(10.0686,–0.0787,–0.0205)
B1N8	*Y* umbilical #1	(0.0686,9.9213,–0.0205)
B1N9	*Z* umbilical #1	(0.0686,–0.0787,9.9795)
B1N10	*X* umbilical #2	(9.9314,–0.0787,–0.0205)
B1N11	*Y* umbilical #2	(–0.0686,9.9213,–0.0205
B1N12	*Z* umbilical #2	(–0.0686,–0.0787,9.9795)

Table 2. Node definitions of TREETOPS STABLE body #2.

Node	Description	Location in Body Coordinates (meter)
B2N1	CM of body #2	(0.004,–0.020,0.067)
B2N2	Origin of body #2 coordinate	(0,0,0)
B2N3	Position detector #1	(0.139,0,0)
B2N4	Accelerometer #1	(0.0411,0.0942,0.0754)
B2N5	Actuator #1	(0,0.1433,0.0423)
B2N6	Position detector #2	(–0.139,0,0)
B2N7	Actuator #2	(–0.1218,-0.1735,0.0423)
B2N8	Accelerometer #3	(–0.0582,–0.1696,0.0754)
B2N9	Position detector #3	(0,–0.139,0)
B2N10	Accelerometer #5	(0.0582,–0.1696,0.0754)
B2N11	Actuator #3	(0.1218,–0.1735,0.0423)
B2N12	Umbilical #1	(0.0686,–0.0787,–0.0205)
B2N13	Umbilical #2	(–0.0686,–0.0787–0.0205)
B2N14	Accelerometer #2	(0,0.0942,–0.0206)
B2N15	Accelerometer #4	(–0.0918,–0.1388,–0.0206)
B2N16	Accelerometer #6	(0.0918,–0.1388,–0.0206)

Table 3. Hinge definitions of STABLE TREETOPS model.

Hinge	Connecting Nodes	No. of DOF	L1_in–L1_out	L3_in–L3_out
1	B0N0–B1N2	3RDOF, 3TDOF	(1,0,0)–(1,0,0)	(0,0,1)–(0,0,1)
2	B1N6–B2N1	3RDOF, 3TDOF	(1,0,0)–(1,0,0)	(0,0,1)–(0,0,1)

B. STABLE Sensors Model

STABLE has six QA–2000 accelerometers on the floating platform to measure acceleration at the attached nodes. This accelerometer was modeled as TREETOPS ACCELEROMETER (AC) sensor that measures the acceleration of body at the specified node in the specified direction. Therefore, six AC sensors are attached on nodes #4, #8, #10, #14, #15, and #16 of body #2. STABLE has three position sensor assemblies to measure the relative position errors between the floating platform and locker base at three position sensor locations. The measured position errors are sent to the digital computer to compute the position error at the actuator gap using the derivation in appendix A. The relative displacement at the gap is the input to the position control law. Each STABLE position sensor assembly consists of a laser attached on the platform and an image detector attached on the locker base. The image detector measures two orthogonal displacements projected on the detector by the laser.

Since there is no built-in TREETOPS sensor corresponding to the STABLE position sensor assembly, a mathematical model of a corresponding position sensor assembly was developed using the TREETOPS POSITION VECTOR (P3) sensor and STAR (ST) sensor. For example, to model the STABLE position sensor assembly at #1 position, a P3 sensor is added on the laser location of the platform to measure three displacement components between the laser attached on the platform and the image detector attached on the locker base, i.e., (x_{p1}, y_{p1}, z_{p1}). Two ST sensors are also added at the laser location of the platform and the detector location of the locker base to measure two relative rotational angles of the laser with respect to the detector about z and y axis, i.e., $(\theta_{1z}, \theta_{1y})$. Then, the output of the TREETOPS position sensor #1 corresponding to the STABLE position sensor assembly #1 can be given by

$$y_1 = -y_{p1} + |x_{p1}| * \tan\theta_{1z} \quad , \tag{1}$$

$$z_1 = z_{p1} - |x_{p1}| * \tan\theta_{1y} \quad . \tag{2}$$

Similarly, the outputs of the TREETOPS STABLE position sensor #2 and #3 can be given by

$$y_2 = y_{p2} - |x_{p2}| * \tan\theta_{2z} \quad , \tag{3}$$

$$z_2 = z_{p2} - |x_{p2}| * \tan\theta_{2y} \quad , \tag{4}$$

$$y_3 = -x_{p3} + |y_{p3}| * \tan\theta_{3z} \quad , \tag{5}$$

$$z_3 = z_{p3} - |y_{p3}| * \tan\theta_{3x} \quad . \tag{6}$$

Although not part of the STABLE flight hardware, for the purpose of performance evaluation, one P3 sensor is attached on the CM of body #1 (B1N1) to measure the relative movement of the CM of the platform with respect to the locker base. Also, two IMU SENSOR (IM) sensors are used to measure the Euler angles of local frames of bodies #1 and #2. These sensors are summarized in table 4.

Table 4. Definition of TREETOPS STABLE sensors model.

Sensor ID No. (Type)	Measurement Quantity	Location (Direction)
SE 101 (AC)	Acceleration #1	B2N4 (1,0,0)
SE 102 (AC)	Acceleration #2	B2N14 (0,0,1)
SE 201 (AC)	Acceleration #3	B2N8 (–0.707,0.707,0)
SE 202 (AC)	Acceleration #4	B2N15 (0,0,1)
SE 301 (AC)	Acceleration #5	B2N10 (–0.707,–0.707,0)
SE 302 (AC)	Acceleration #6	B2N16 (0,0,1)
SE 401 (ST)	$\theta_2 \& \theta_3$ of laser #1	B2N3 (0,1,0) & (0,0,1)
SE 402 (ST)	$\theta_2 \& \theta_3$ of detector #1	B1N3 (0,1,0) & (0,0,1)
SE 501 (ST)	$\theta_2 \& \theta_3$ of laser #2	B2N6 (0,1,0) & (0,0,1)
SE 502 (ST)	$\theta_2 \& \theta_3$ of detector #2	B1N4 (0,1,0) & (0,0,1)
SE 601 (ST)	$\theta_1 \& \theta_3$ of laser #3	B2N6 (1,0,0) & (0,0,1)
SE 602 (ST)	$\theta_1 \& \theta_3$ of detector #3	B1N4 (1,0,0) & (0,0,1)
SE 701 (P3)	$X_{p1}.Y_{p1}.Z_{p1}$	(B1N3)–(B2N3)
SE 801 (P3)	$X_{p2}.Y_{p2}.Z_{p2}$	(B1N4)–(B2N6)
SE 901 (P3)	$X_{p3}.Y_{p3}.Z_{p3}$	(B1N5)–(B2N9)
SE 911 (P3)	Relative movement of body #2 CM w.r.t body #1	(B1N6)–(B2N1)
SE 921 (P3)	Movement of body #1 CM	(B1N6)–(B2N1)
SE 912 (IM)	Euler angles of body #2 frame	B2N1
SE 922 (IM)	Euler angles of body #1 frame	B1N2

C. STABLE Actuator Model

The STABLE has three MDA dual-axis actuators which generate two orthogonal forces and are modeled as two TREETOPS JET (J) actuators. The actuator applies a force at the node of the platform where the actuator is attached. Each JET actuator gives constant force that is defined using a FUNCTION GENERATOR (FU) at the specified node to the specified direction. Therefore, six JET actuators are attached on nodes #5, #7, and #11 of body #2. For the purpose of performance analysis, a disturbance can be given by applying a force on the CM of body #1 using a separate JET actuator. These actuators are summarized in table 5.

Table 5. Definition of TREETOPS STABLE actuators model.

Actuator ID No. (Type)	Measurement Quantity	Location (Direction)
AC 101 (J)	Actuator force #1	B2N5 (1,0,0)
AC 102 (J)	Actuator force #2	B2N5 (0,0,1)
AC 201 (J)	Actuator force #3	B2N7 (–0.707,0.707,0)
AC 202 (J)	Actuator force #4	B2N7 (0,0,1)
AC 301 (J)	Actuator force #5	B2N11 (–0.707,–0.707,0)
AC 302 (J)	Actuator force #6	B2N11 (0,0,1)

D. STABLE Controller Implementation

The high performance characteristics of the isolator are the result of active feedback loops involving actuators, sensors, and electronics. The isolated platform is controlled by means of six independent control channels, one for each actuator force direction. Each STABLE control channel consists of one fast inner acceleration control loop and one slow outer position control loop, as described in section II.

In order to implement this STABLE controller in the TREETOPS dynamics model, three TREETOPS control modules (CBDC, USDC, and USCC) were used. The inner acceleration controller loop was modeled using continuous block diagram controller (CBDC) and the outer position controller loop was modeled using user-defined discrete controller (USDC) subroutine. The user-defined continuous controller (USCC) subroutine was used to connect the inner acceleration controller loop and the outer position controller loop. The USCC and USDC subroutines are documented in reference 3.

1. Position Control Loop

The STABLE position PID controller was implemented in the TREETOPS STABLE model using a USDC subroutine.[3] This USDC routine generates the acceleration command, based on position error, and prints out the intermediate results for the purpose of performance analysis. This routine also provides a procedure that determines the output of the TREETOPS position sensor model corresponding to the STABLE position sensor assembly using equations (1)– 6). The relative displacements at the actuator gap are computed from the position sensor measurements in a two-step process. First the displacements of the platform CM $(x_{cg}, y_{cg}, z_{cg}, \theta_{x_{cg}}, \theta_{y_{cg}}, \theta_{z_{cg}})$ are determined and then the displacements at the actuator gaps are determined, given the location of the CM, the sensors, and the actuators. The relationships between the outputs of STABLE position sensors, the relative displacements of the platform CM, and the relative displacements at the actuator gaps are derived in appendix A. The discrete position control loop computes an acceleration command which will force the position error at the actuator gap to tend to be zero.

2. Acceleration Control Loop

Prior to implementing the acceleration control law in CBDC, the USCC sets the control gain and performs part of the acceleration control law computation. Inputs to the USCC are the high or low gain flag (determined by the mode switching logic in the position control law), acceleration command from the position loop ($\ddot{x}_c$), and the measured acceleration ($\ddot{x}$). USCC is used to select and output the proper (high or low) acceleration control gain (K_A) and products ($K_A * \ddot{x}$) and ($K_A * \ddot{x}_c$). These quantities are output for use by CBDC. (In the flight system, the acceleration command and measurement are summed to form the error signal which is multiplied by the acceleration gain and processed by the analog acceleration control law. To realize this operation in TREETOPS controller block structure, the gain is multiplied by acceleration command and measurement prior to summation.)

The STABLE inner acceleration controller has six independent channels for six actuator forces and is modeled using TREETOPS CBDC. STABLE employs an analog single-input/single-output acceleration control architecture. Based on the collocated acceleration measurement, a control force is computed to reduce the inertial motion of the platform. Each channel has the same control law and continuously determines control force to compensate for an acceleration error at the actuator attach point. CBDC generates a control force for each actuator force direction by summing the outputs of USCC ($K_A * \ddot{x}$) and ($K_A * \ddot{x}_c$)and processing the error signal by the transfer function representing the analog control circuitry.

For the TREETOPS model, a total of thirty inputs, five for each channel, are read into CBDC. The inputs of each channel are two FUNCTION GENERATORs (FU) that provide a dc bias and white noise acceleration component, an acceleration measured by the AC sensor, and two outputs of USCC, $K_A * \ddot{x}$ and $K_A * \ddot{x}_c$. CBDC generates a control force for each actuator output direction by computing $(-K_A * \ddot{x} - K_A * \ddot{x}_c)$ and processing the error signal by the transfer function representing the analog control circuitry. This CBDC generates twelve outputs, two for each channel—the actuator control force and the total acceleration from acceleration control loop.

IV. SIMULATION RESULTS

This subsection describes numerical results of STABLE stability and attenuation performance analysis obtained from TREETOPS simulation. The input file of the STABLE TREETOPS simulation is documented in reference 3. For the stability analysis, two cases are considered: One is to check stability of the STABLE system by measuring the transient response of the platform with given initial movement of platform and the other is to check stability of the STABLE system by measuring the transient response of the platform with a given pulse-type disturbance on base. The attenuation performance analysis was done to determine the acceleration attenuation curve by measuring the acceleration at the platform CM due to the various frequencies of sinusoidal disturbances given to the base. Mass properties of the STABLE platform are described in table 6.

Table 6. Mass properties of the STABLE platform.

Mass (Kg)	12.646
$I_{xx}, I_{yy}, I_{zz}, I_{xy}, I_{yz}$ $(Kg\text{–}m^2)$	0.167, 0.108, 0.179, 0, 0, 0

As explained in section III, the umbilicals are modeled as combinations of linear and quadratic spring devices. Based on the measured spring stiffness, the linear spring stiffness coefficients used for TREETOPS STABLE model are 18 N/m in the positive X-axis direction, 13.5 N/m in the positive Y-axis direction, and 20 N/m in the positive Z-axis direction. The quadratic spring stiffness coefficient used for TREETOPS STABLE model is -672 N/m^2 to the positive Z-axis direction.

Final control parameters used for the acceleration controller and PID position controller of the flight STABLE system were determined through iterative design and performance simulation and are summarized in table 7. In figure 4, K_{IL} and K_{IH} correspond to the low and high gain mode values for K_I, respectively. Similarly, K_{LL} and K_{LH} correspond to the low and high gain mode values for K_L, respectively. RH and RL are parameters which specify the mode switch regions in figure 5.

Table 7. STABLE control parameters.

Control Parameters	Low Gain Mode	High Gain Mode
K_A(N*sec²/m)	5.5e+4	5.5e+4
Lead-lag filter Transfer function	$\frac{1}{10}\left(\frac{s+2\pi*10}{s+2\pi}\right)$	$\frac{1}{10}\left(\frac{s+2\pi*10}{s+2\pi}\right)$
K_D(1/sec)	8.8e-2	2
K_P(1/sec²)	4e-3	4e-1
K_I(1/sec³)	4e-5	4e-2
Max. C_{il} (μg)	20	-
RL (mm)	2	-
RH(mm)	-	8
LSB (μg)	0.2	10
ΔC_{il} (μg)	10	-
K_L	2	1
T_S	0.1	0.1
N_S	-	100

A. Case 1: Transient Response Analysis With Initial Displacement

In order to investigate the stability of the STABLE control system with acceleration and position control, the STABLE platform was initially displaced from the nominal resting position by 10 mm in each axis direction. Accelerometer bias and white measurement noise are added to the accelerometer outputs to represent the hardware characteristics of the STABLE accelerometers. High gain mode was set initially and the transient response was then calculated from the TREETOPS simulation. The acceleration biases for the six accelerometers were chosen arbitrarily for this simulation, as shown in table 8.

Table 8. Acceleration biases of six accelerometers.

Acc. Bias	A11	A13	A21	A23	A31	A33
μg	105	-155	85	-125	25	115

The white acceleration measurement noise was generated with random numbers multiplying the following transfer function implemented in CBDC:

$$T_{whi} = \frac{K\omega_n^2(s+a)}{a(s^2+2\xi\omega_n s+\omega_n^2)}, \tag{7}$$

where K=2×10^{-5} m/sec^2, a=2π(20) rad/sec, ω_n=2π(100) rad/sec, and ξ=0.85.

Numerical simulation results of the STABLE transient response analysis are shown in figures 7–14. The gains of the PID controller were selected based on the switching logic and are shown in table 7.

Figure 7 shows the following time responses: The output of the six PID position controller's channels; the accelerations A11, A21, and A31 are parallel to the direction of accelerometers #1, #3, and #5, respectively; and the accelerations A13, A23, and A33 are in the Z-axis direction parallel to the direction of accelerometers #2, #4, and #6, respectively. As shown in this figure, high gain mode was initially active for about 40 sec and when all six channels satisfied the low gain criteria for more than N_s time samples simultaneously, the position controller changed into low gain mode to get precise control of position. It should be noted that all six channels show outputs with equal magnitude and opposite signs of the accelerometer biases given in table 8.

Each channel of the position controller has two output signals—coarse acceleration (PC) quantized with 10 μg least significant bits (LSB) and fine acceleration (PF) quantized with 0.2 μg LSB. In figure 8, the coarse and fine channels are designated PCij and PFij, respectively. Defining A_1 and A_2 be acceleration output without and with quantization, respectively, the equation of quantization may be given as follows:

$$A_2 = int\left[\left(|A_1| + \frac{LSB}{2}\right)/LSB\right] * LSB * sign(A_1) \quad . \tag{8}$$

The sum of PF and PC is the output of the PID position controller and is fed back to the acceleration controller implemented in CBDC at every sampling time. These results are shown in figures 8 and 9.

Detailed outputs of the sixth channel of the position controller are presented in figure 10. In this figure, the first row of plots show position error, position error rate, and integrated position error in the Z-axis direction at the gap of actuator #3. Multiplying these error signals by the PID gains given in table 7 yields cp, cr, ci_low, and ci_high. The coarse acceleration output (PC) is the sum of cp, cr, and ci_high. The fine acceleration output (PF) is the sum of cp, cr, and ci_low. The last row of plots shows indication of PID position high or low gain mode.

Figure 11 shows the outputs of six accelerometers: A11, A13, A21, A23, A31, and A33 are the measured accelerations of the accelerometers #1, #2, #3, #4, #5, and #6, respectively. It is noted that the acceleration controller immediately senses abrupt changes of several hundred microgravity accelerations and reduces the acceleration levels to the given output noise level of accelerometer. The acceleration command from the position controller results from the position controller command to move the STABLE platform from the initially displaced position to the nominal rest position; therefore, the acceleration controller is operating as designed.

Figure 12 shows the position errors measured by the STABLE position sensors described in section II. In figure 12, $Y1$ and $Z1$, $Y2$ and $Z2$, and $Y3$ and $Z3$ are Y-axis and Z-axis directional position

errors of the STABLE position sensors #1, #2, and #3, respectively. It is shown that the PID position controller brings down position error of the STABLE platform from initial 10 mm to zero mm in a timely manner.

The controller position errors at the CM of the STABLE platform, shown in figure 13, are calculated using equations (11)–(21) in appendix A together with the position errors measured by position sensors. To check the validity of equations (11)–(21), the position errors at the CM of the STABLE platform were obtained from TREETOPS' built-in position sensor at the CM of STABLE platform and hinge #1's output, and plotted using the dotted line in figure 13. These results confirm the validity of equations (11)–(21) and the effectiveness of the STABLE PID position controller.

Figure 14 shows the position errors at the actuators' gap, determined using equation (28) in appendix A. In this figure, outer dotted lines denote RH (±8 mm) and inner dotted lines denote RL (±2 mm), and these results verify the switching logic for the high/low gains of the PID position controller explained in section II.

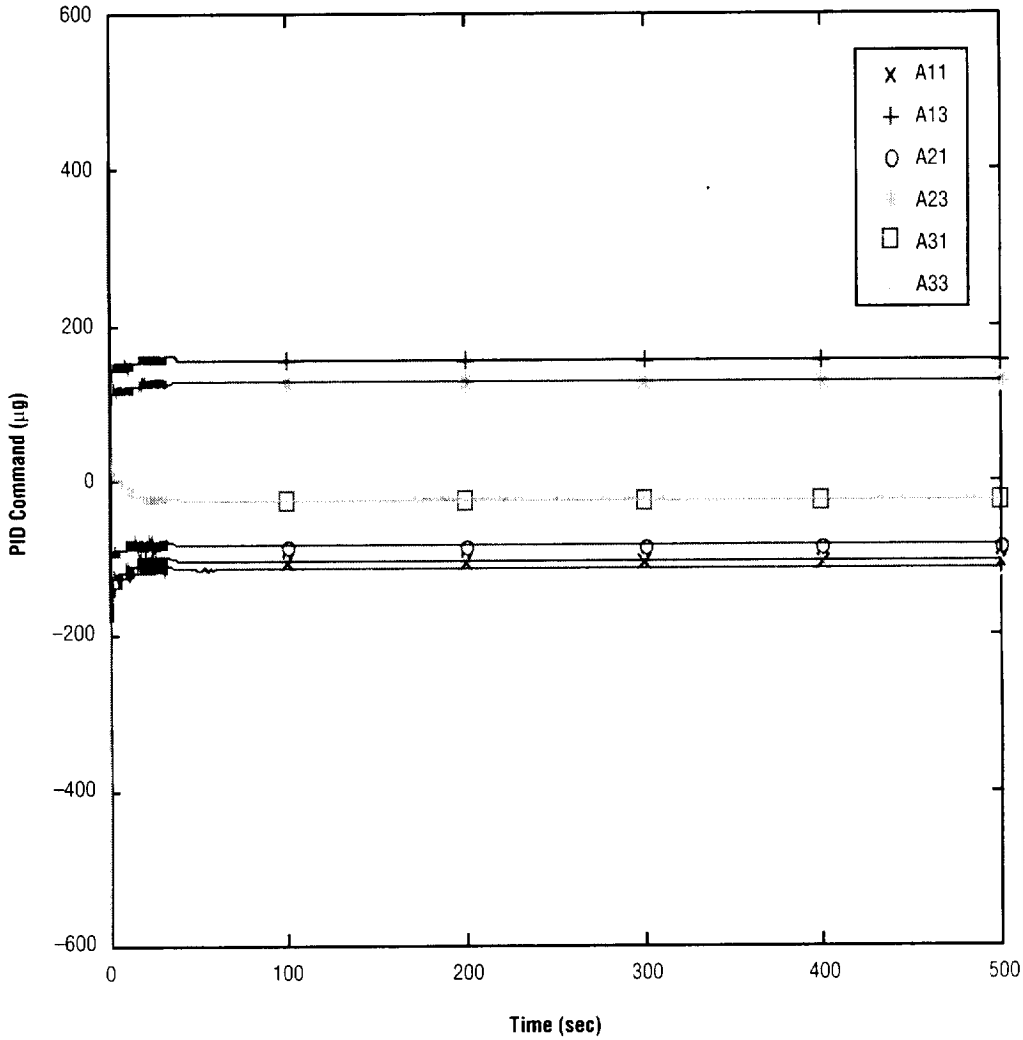

Figure 7. PID position controller output with initial displacement.

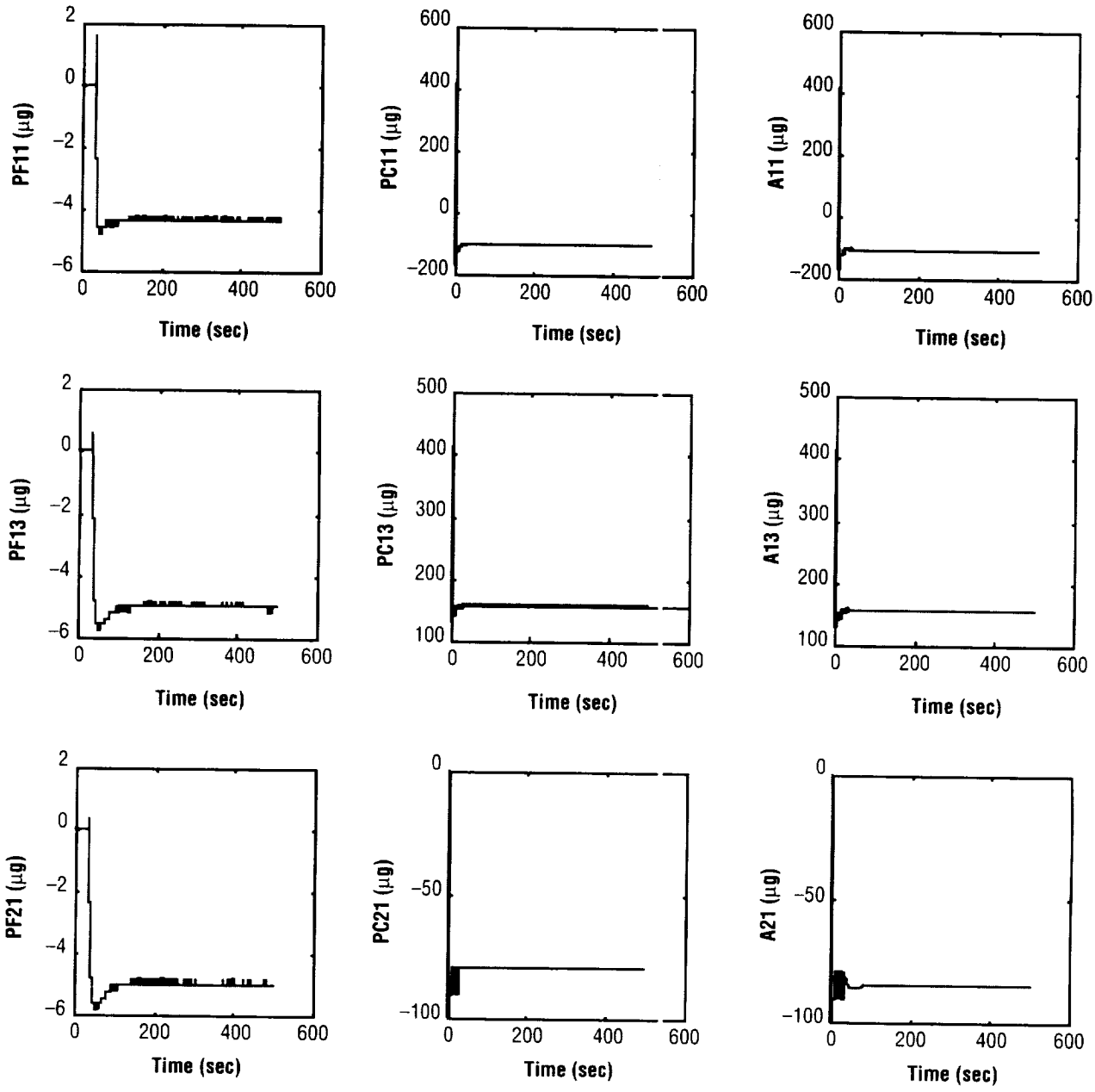

Figure 8. Detailed PID position controller output with initial displacement.

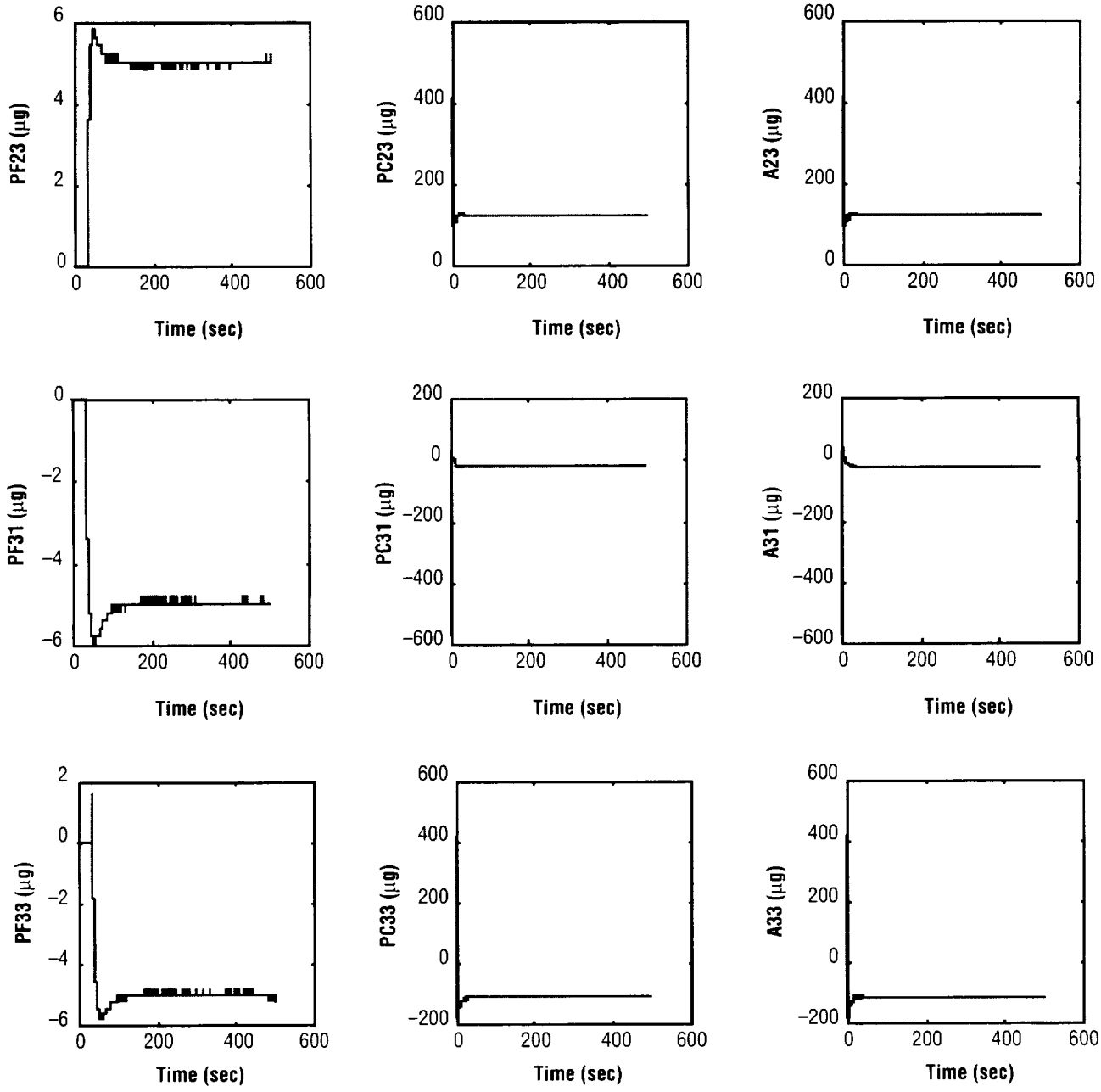

Figure 9. Detailed PID position controller output with initial displacement (Continued).

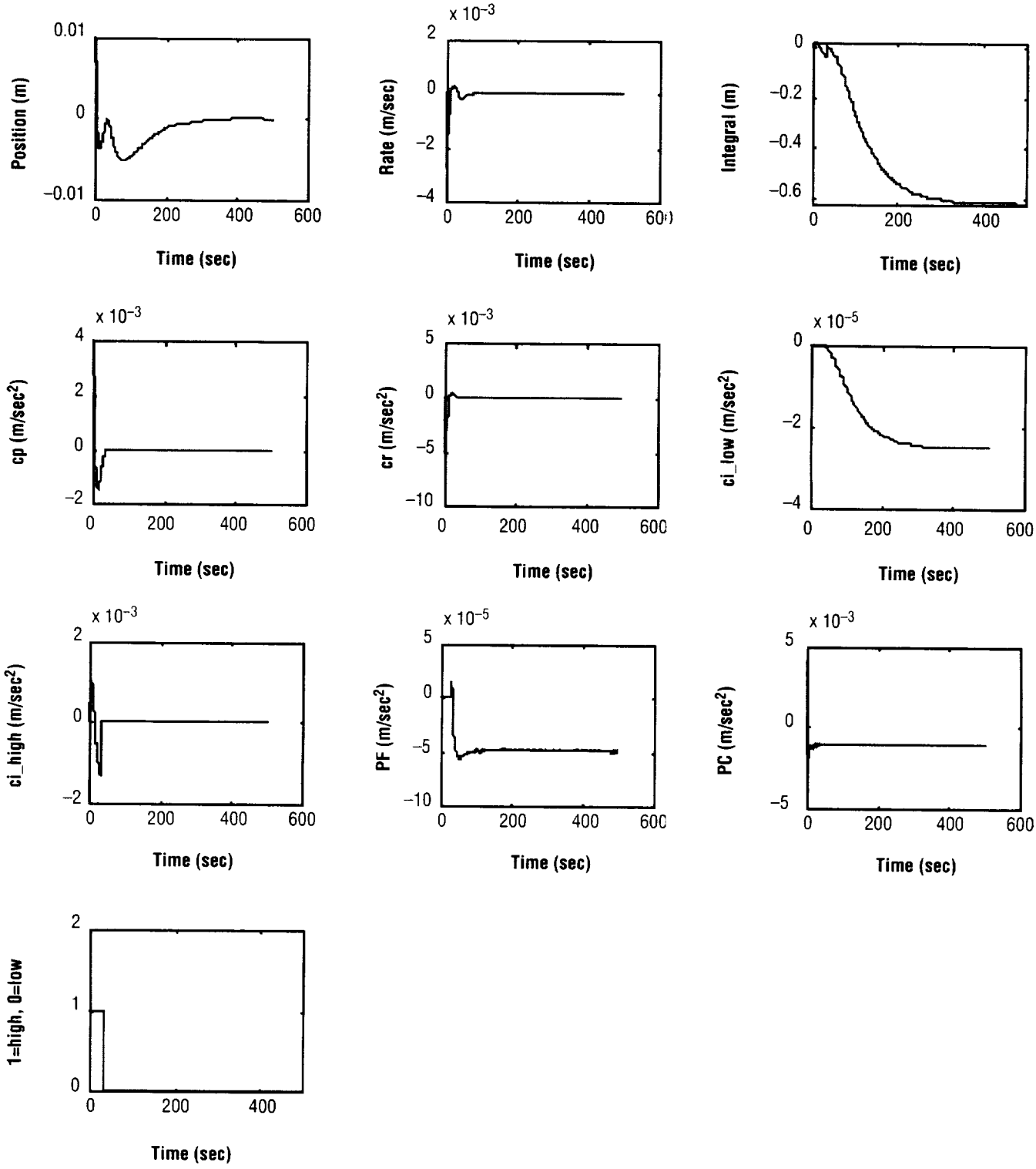

Figure 10. Detailed PID position controller output of sixth channel with initial displacement.

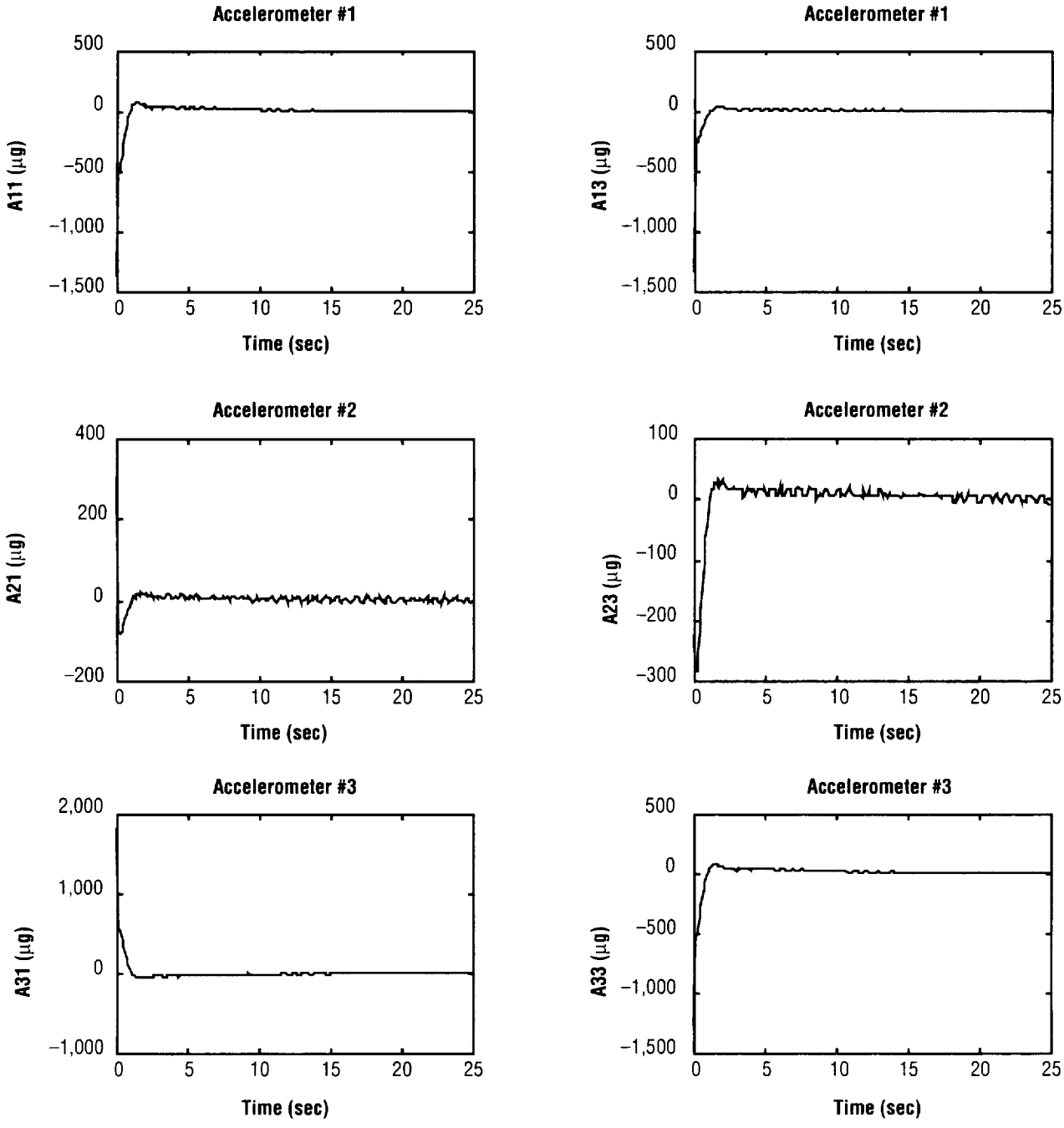

Figure 11. Output of accelerometers with initial displacement.

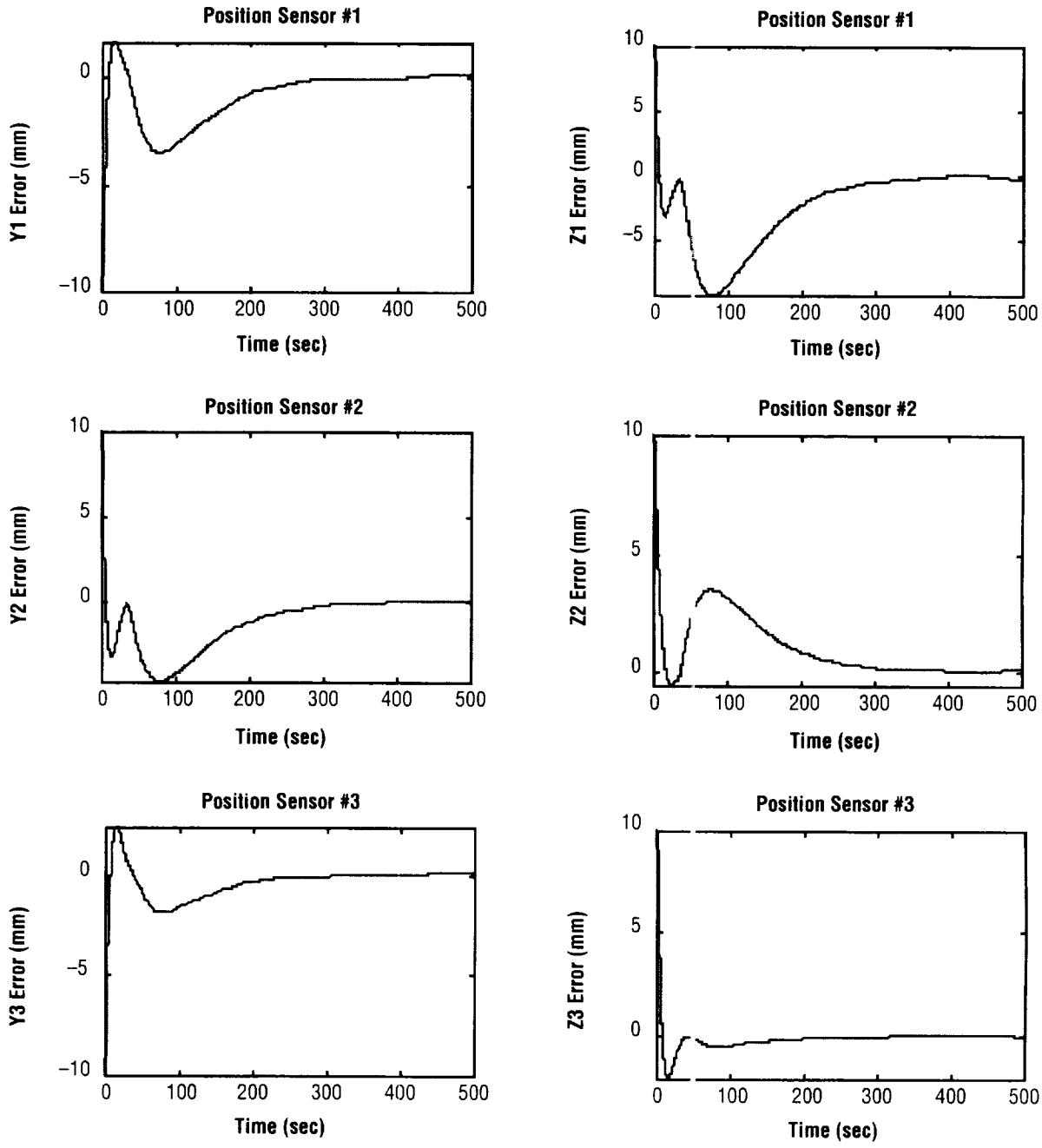

Figure 12. Output of position sensors with initial displacement.

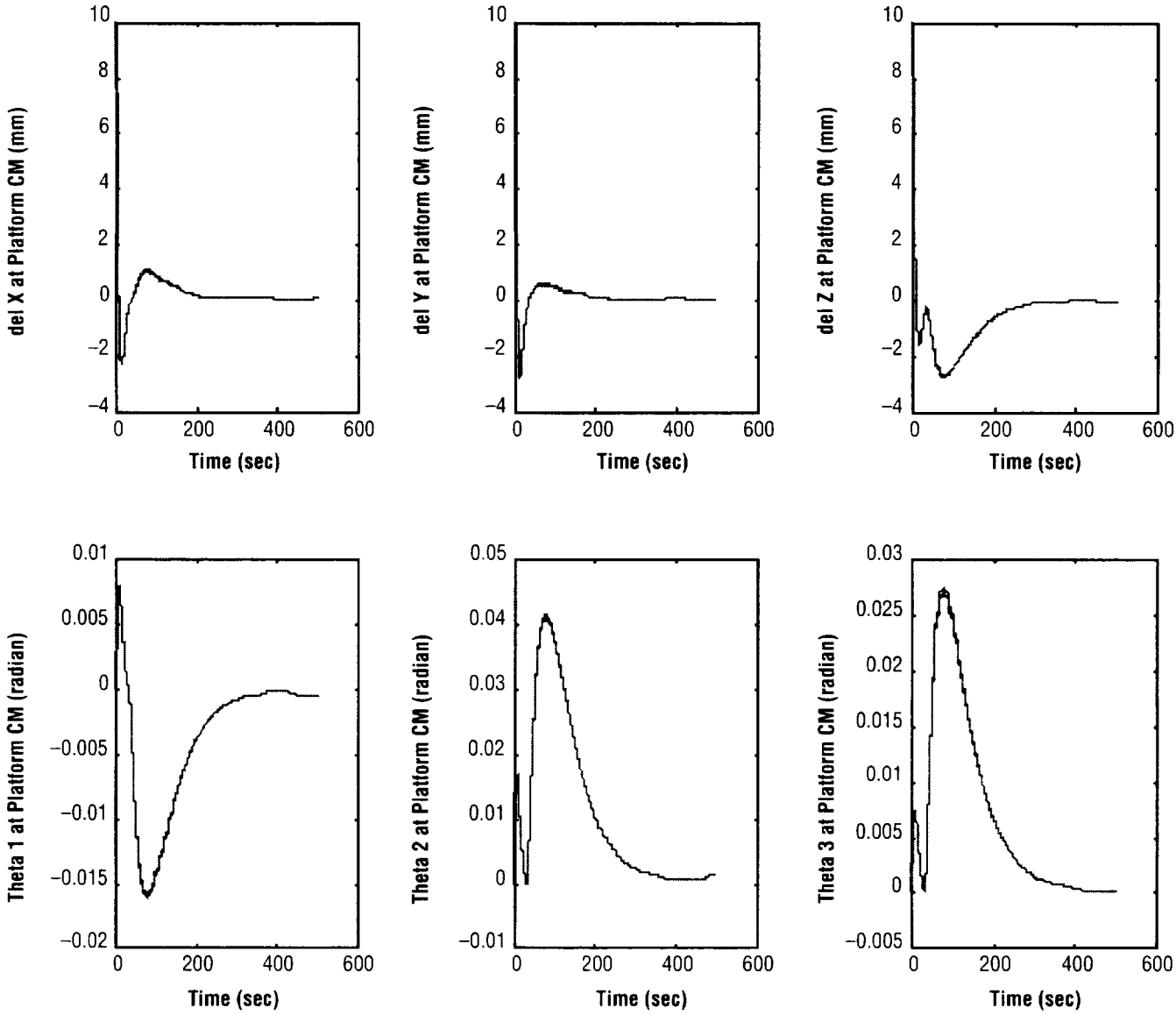

Figure 13. Position error at the CM of STABLE platform with initial displacement.

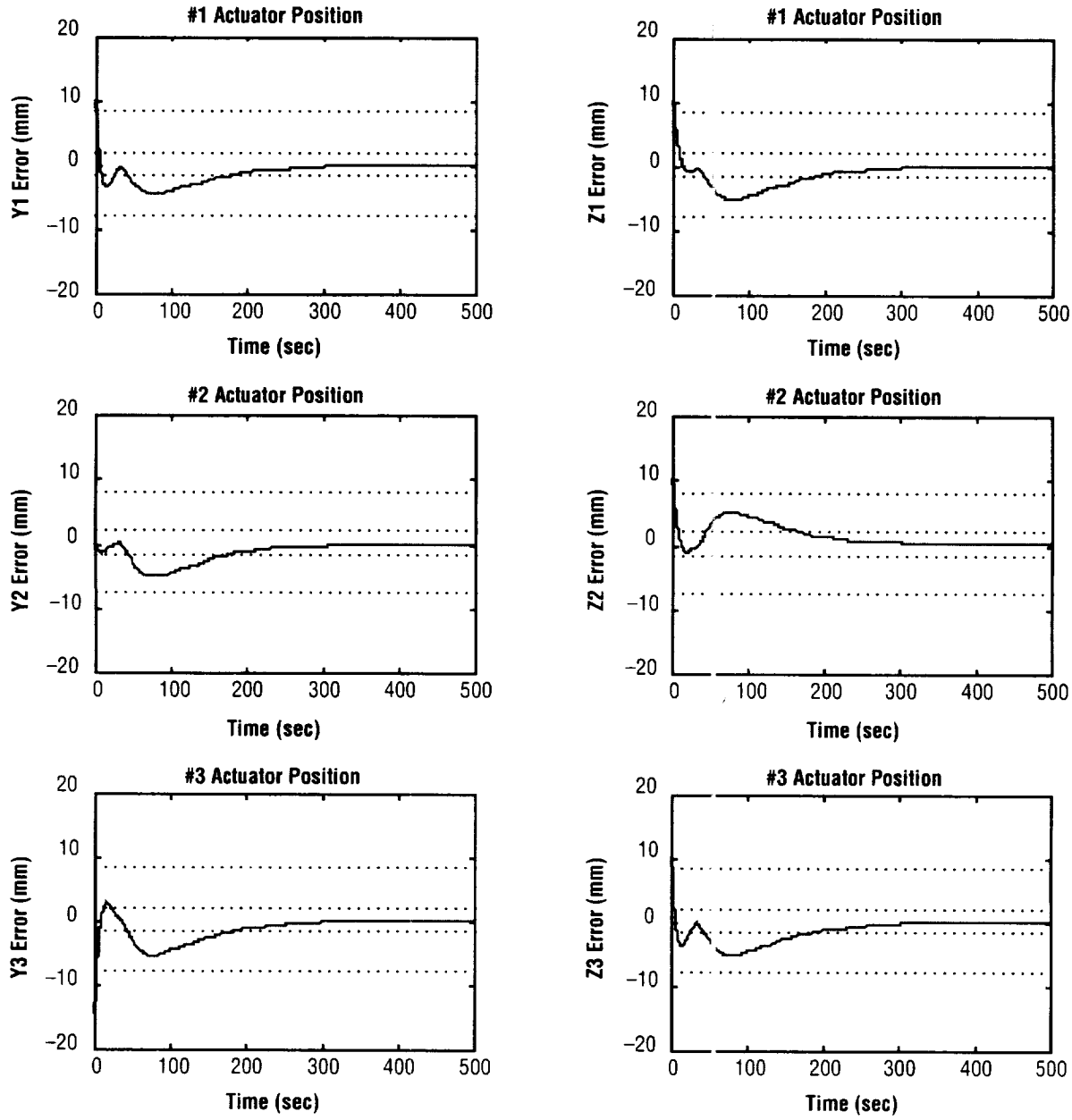

Figure 14. Position error at the center of actuators gap with initial displacement.

B. Case 2: Transient Response Analysis With Initial Excitation

In order to demonstrate how well the STABLE system can overcome sudden disturbance, a 1,000-μg step disturbance input was given to the base of the *Z*-axis direction for 1 sec, and then a transient response analysis was performed using input data tables 7 and 8 with initial low gain mode. The biased acceleration and white noise of the accelerometers used for this simulation are the same as those used in case 1.

The numerical results of this transient response analysis are shown in figures 15–22. Figures 15–17 show the output of the six PID position controller's channels with detailed output of sixth channel of position controller presented in figure 18. Figure 19 shows the measurements of the reference six accelerometers. As shown in these figures, the abrupt disturbance is sensed and the controller shifts from low gain mode into high gain mode immediately. The STABLE controller effectively responds to abrupt input accelerations and reduces the platform acceleration to the noise level of the accelerometers. It is also noted that the low gain mode may be recovered in about 40 sec.

Figure 20 shows the position errors measured by the STABLE position sensors and the position errors at the CM of the STABLE platform are shown in figure 21. Figure 22 shows the position errors at the actuator gap.

C. Case 3: Attenuation Performance Analysis Results

The main objective of the STABLE system is to provide a low acceleration environment across a broad spectrum of frequencies using an active isolation controller. An attenuation performance analysis of the STABLE control system was performed and numerical results are presented in this section. The acceleration attenuation of STABLE system was estimated by measuring the accelerations at the platform CM for given sinusoidal disturbances of various magnitudes and frequencies. For this analysis, the accelerometer bias, accelerometer noise, and initial displacement are not included. The acceleration attenuation curve was determined by taking the ratio of acceleration magnitudes at the platform CM to the given disturbance acceleration magnitudes across the frequency range of 0.001 through 100 Hz. Figure 23 shows the calculated acceleration attenuation curve of the STABLE system. With a break frequency of approximately 0.01 Hz and rolloff of approximately 20 dB/decade, good attenuation is achieved. The slight amplification below 0.02 Hz is a consequence of low frequency acceleration commands produced by the position controller to keep the platform centered in the sway space.

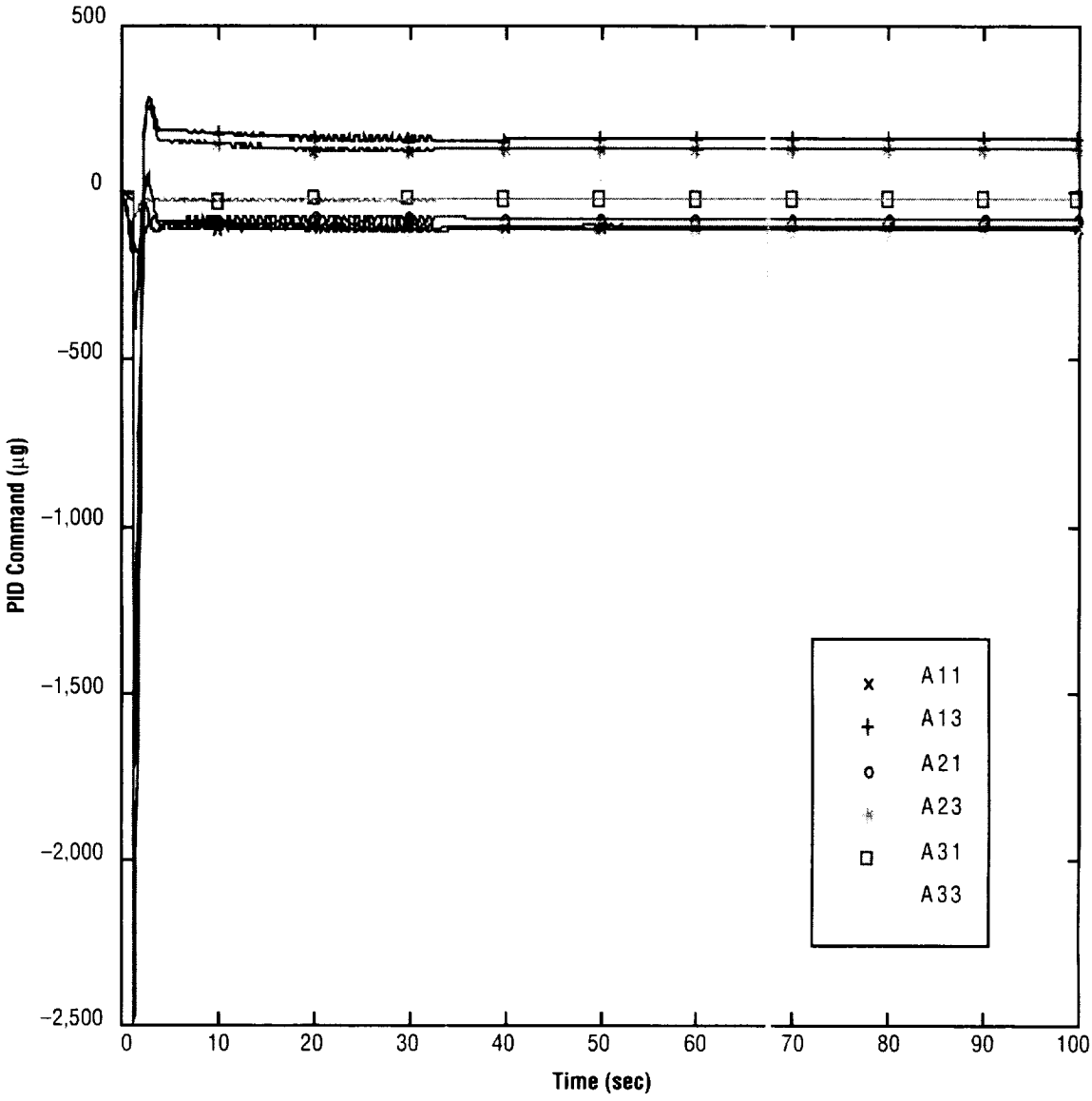

Figure 15. PID position controller output with initial excitation.

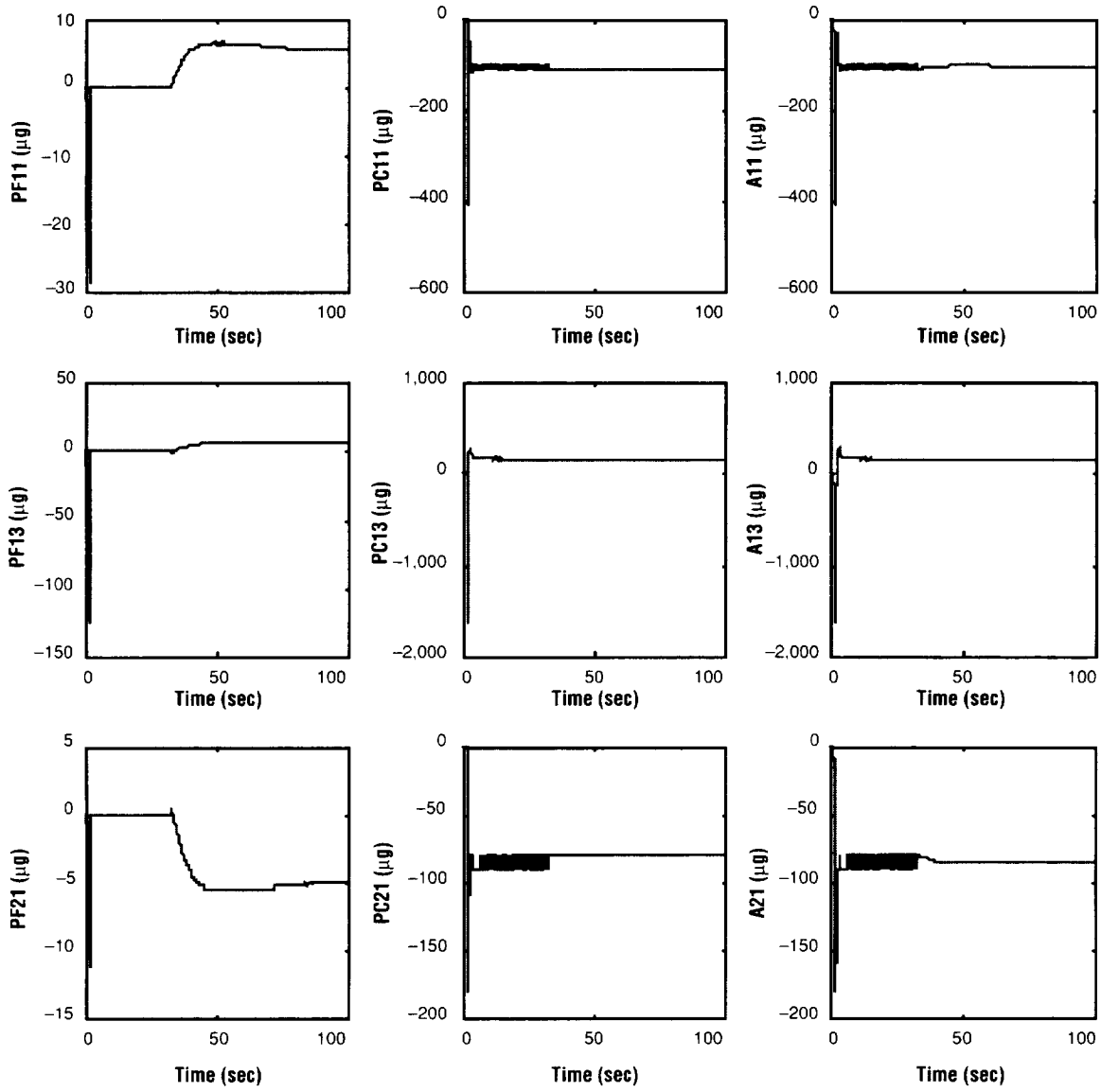

Figure 16. Detailed PID position controller output with initial excitation.

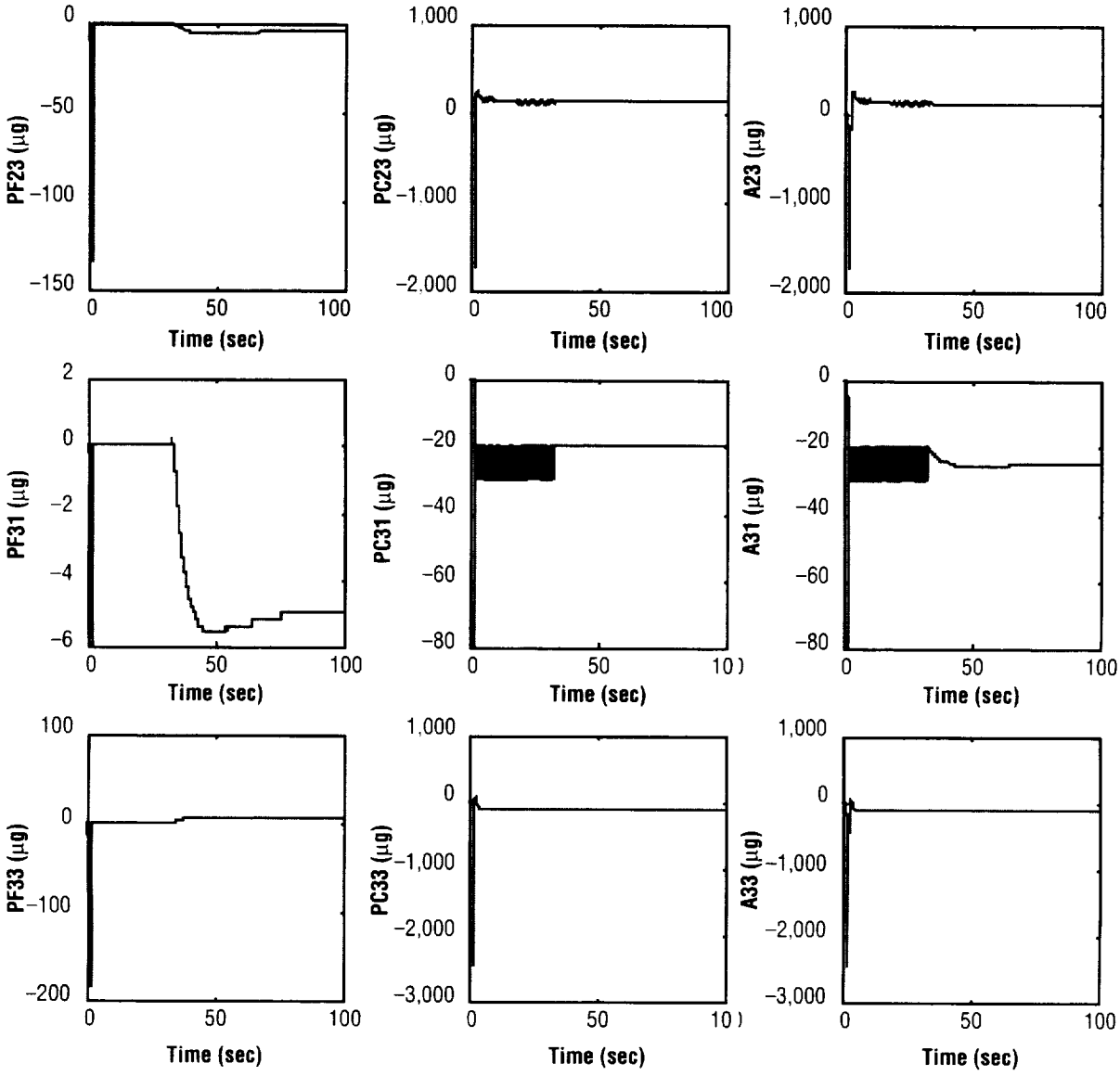

Figure 17. Detailed PID position controller output with initial excitation (Continued).

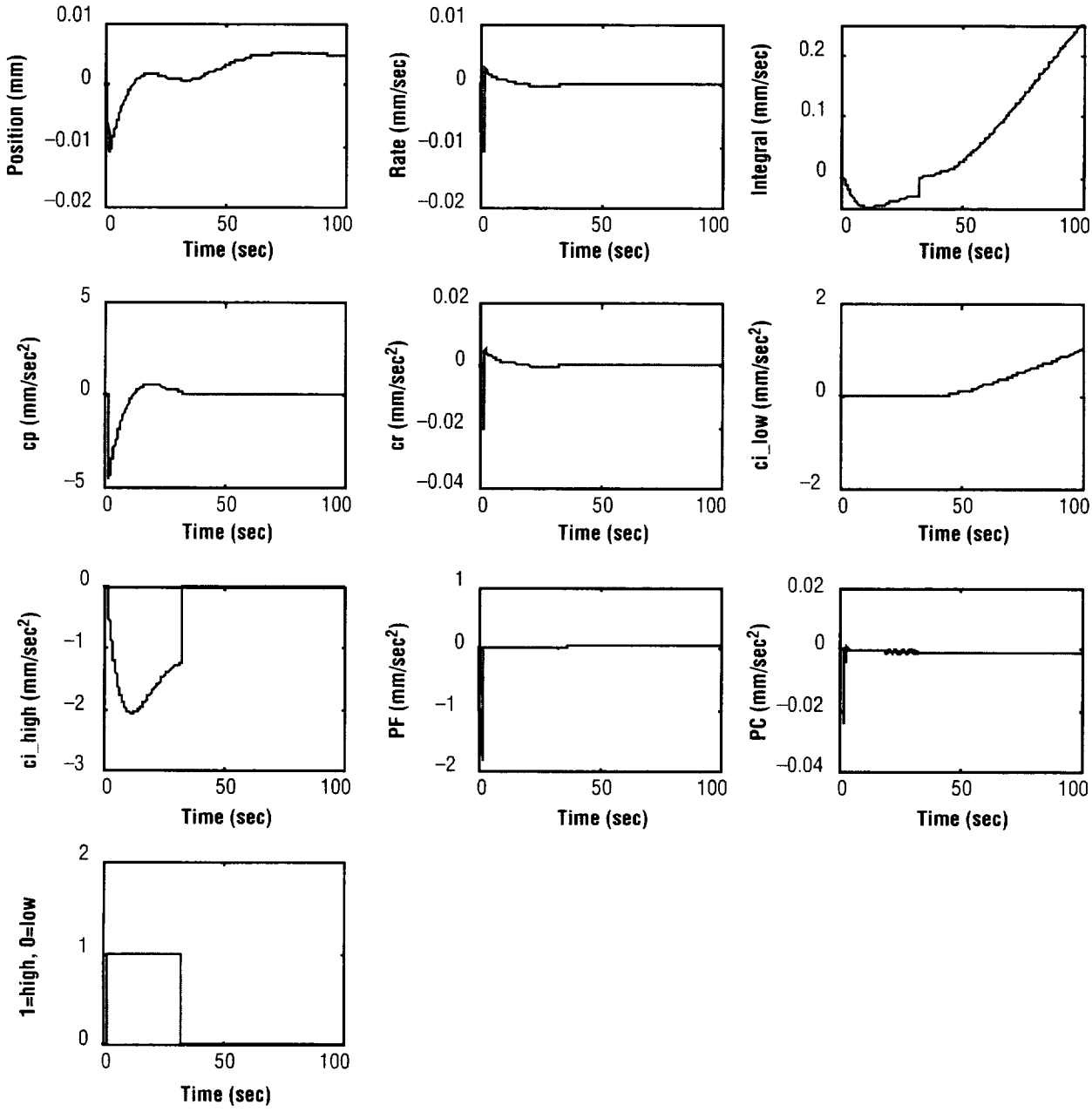

Figure 18. Detailed PID controller output of sixth channel with initial excitation.

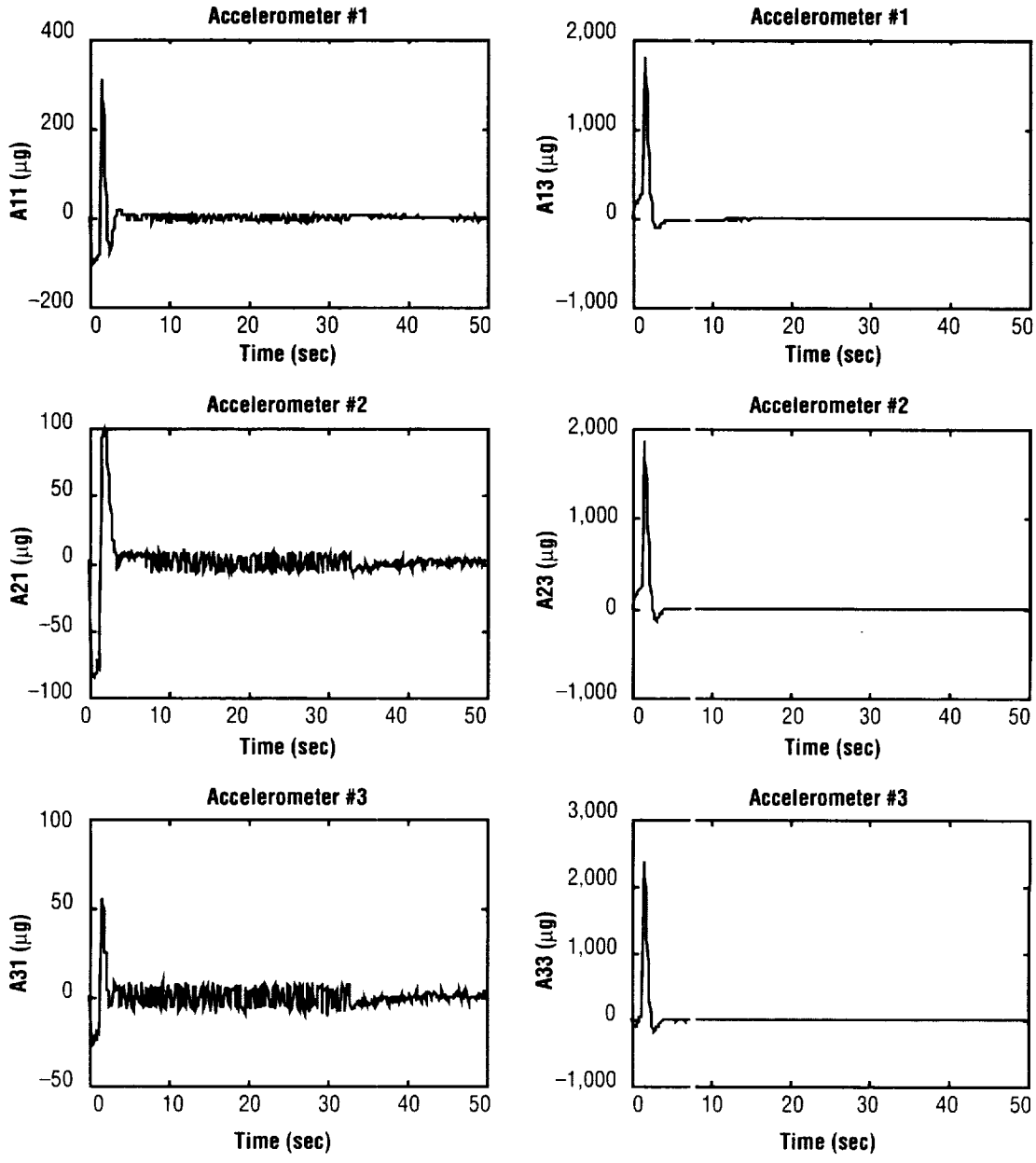

Figure 19. Output of accelerometers with initial excitation.

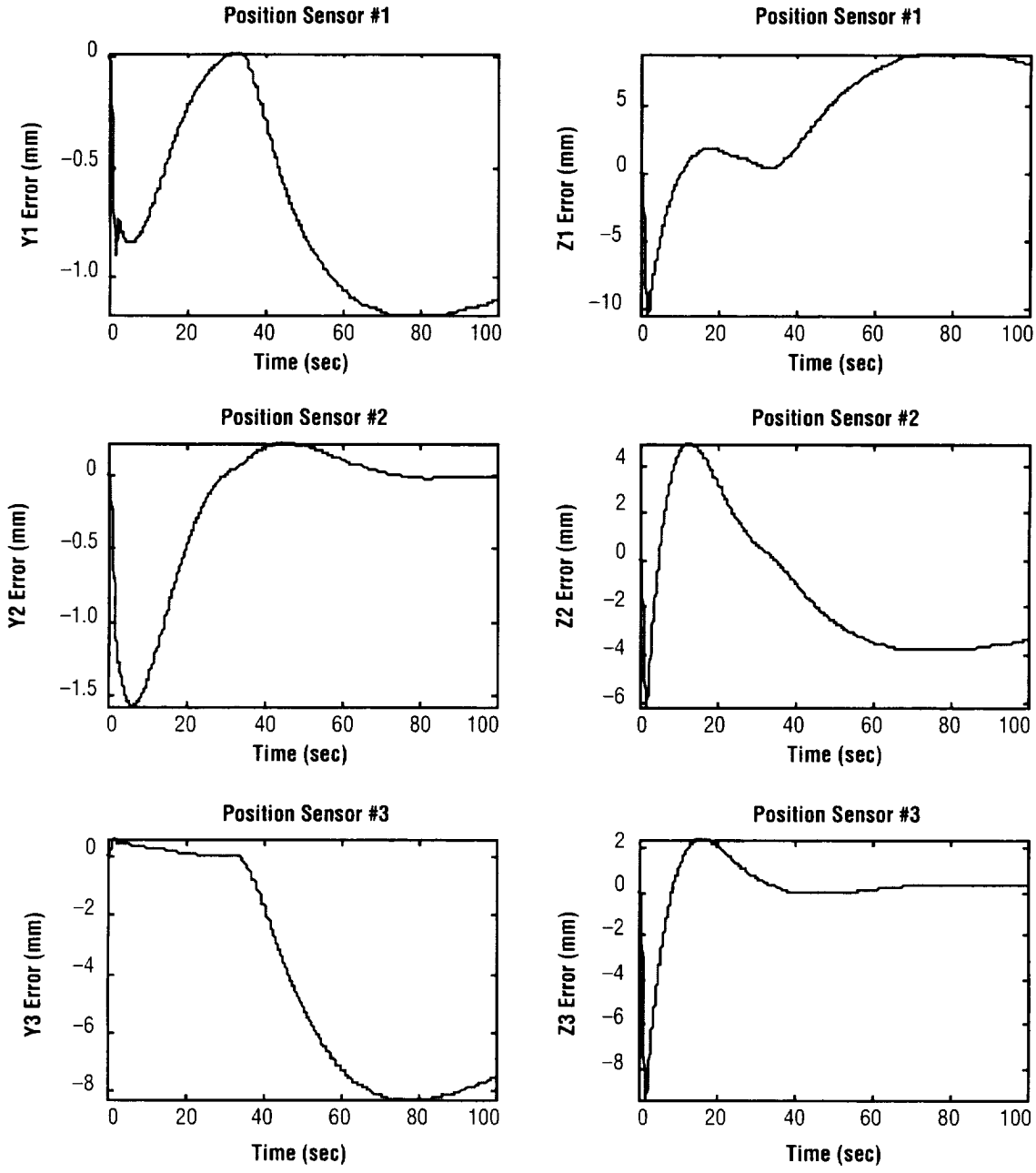

Figure 20. Output of position sensors with initial excitation.

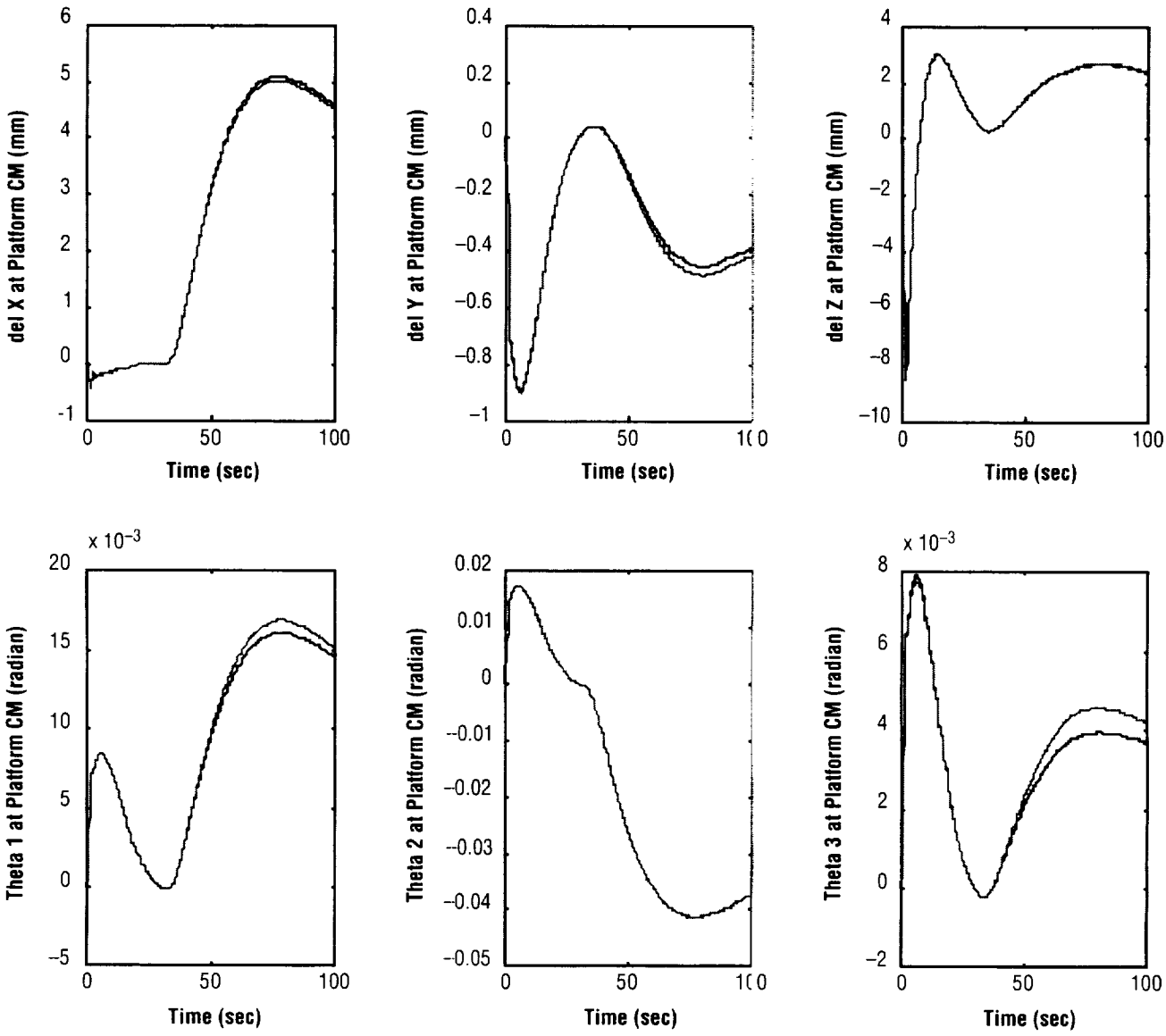

Figure 21. Position error at the CM of STABLE platform with initial excitation.

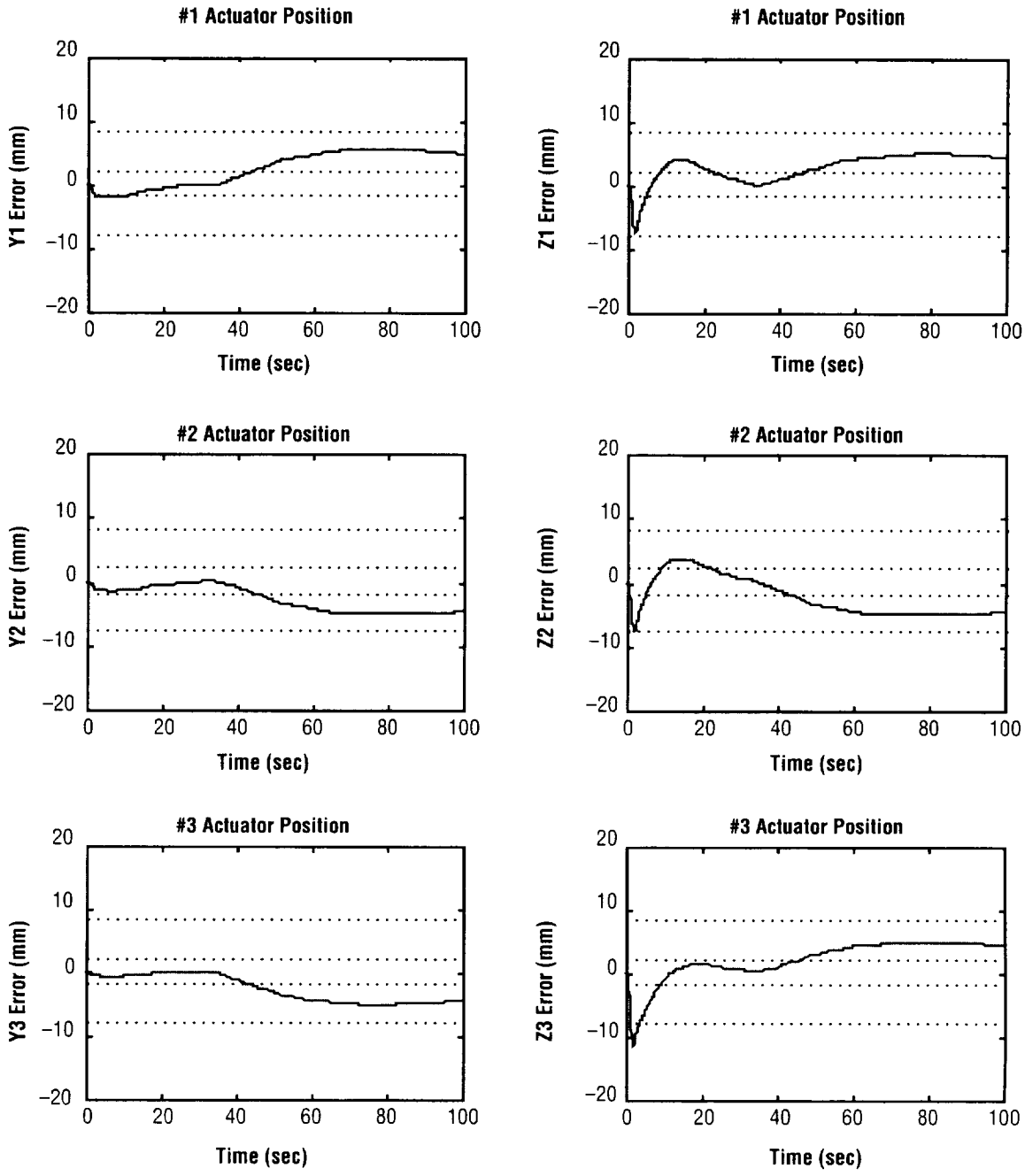

Figure 22. Position error at the center of actuators gap with initial excitation.

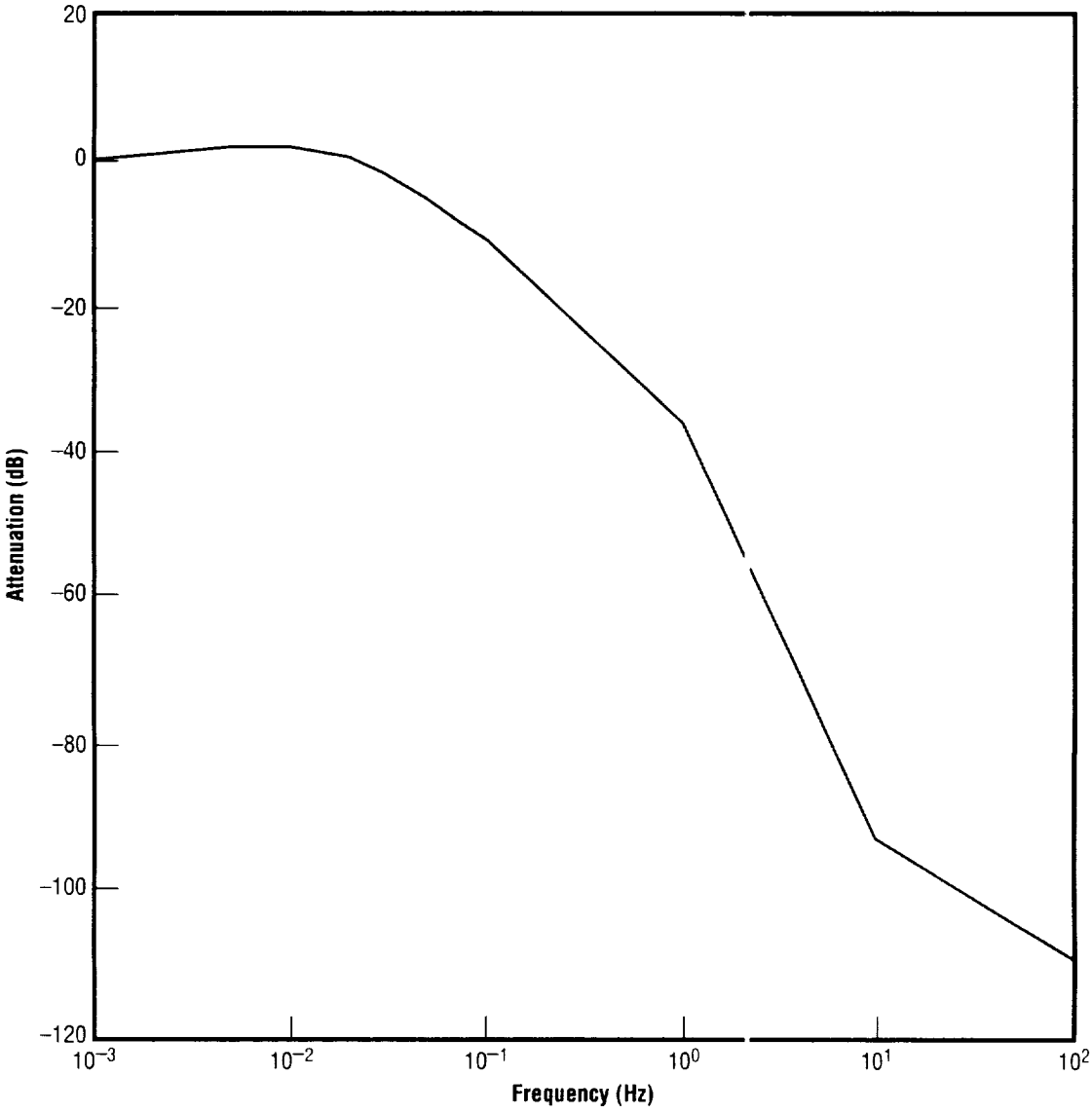

Figure 23. Acceleration attenuation curve of STABLE system.

V. CONCLUSIONS

This report documents the details of the control/dynamics simulation used to design the control laws and define the expected performance of the STABLE isolation system. The multibody simulation tool, TREETOPS, was used to implement the 6 DOF dynamics of the floated platform as well as the dynamical models of all sensors, actuators, and the control algorithms in the software. Where possible, models were based on measured data and transfer functions; and, therefore, the simulation should be a good representation of the actual hardware performance. It should be noted that the performance prediction in terms of an attenuation transfer function does not meet the requirement that was established for STABLE. This was due to a situation in which, because of schedule pressure, it was necessary to use hardware that was designed for another program, hardware whose electronics characteristics forced a compromise in the design of the bandwidth of the position control loop. The results in this report will be compared to flight data and will be published in a separate report.

APPENDIX A—Derivation of Relative Position at the Actuator Gap

Since the six control loops are decoupled and use measurements collocated with the actuators, the input to the position control law is the relative displacement of the isolated platform with respect to the base at the actuator gap and in the direction of actuator force axes. However, the position sensors are located remotely from the actuators in the STABLE configuration. A laser mounted on the isolated platform illuminates a detector fixed on the base to provide a measure of the relative motion. Each detector measures two axes of motion in the plane of the detector, normal to the incident laser beam. These six relative position measurements are used to compute the relative motion at the actuator gaps based on the locations of the actuators, lasers, and detectors through a two-step process. First, the 6-DOF motion of the CM is computed from the sensor measurements and then the resulting displacement at the actuator gaps is determined. The equations defining these two steps are derived in the following sections.

A.1 Center of Mass Relative Displacements

Figure 24 indicates the vectors and coordinate frames used for the computation of the position error projected onto the detector plane of sensor #1 that results from motion of the platform CM, $(x_{cg}, y_{cg}, z_{cg}, \theta_{x_{cg}}, \theta_{y_{cg}}, \theta_{z_{cg}})$. The relative position, as measured by the detector at sensor #i (i=1,2,3), is the projection of the error vector, $\underline{e}_i$, onto the detector plane. The error vector is given by

$$\underline{e}_i = \underline{r}_0 + \underline{r}_{cm} + \underline{\rho} + \underline{S}_i - (\underline{S'}_i + \underline{\Delta}_i) , \tag{1}$$

where the Y frame is fixed in the base such that the center of the detectors lie in the $\underline{Y}_1\,\underline{Y}_2$ plane; the Z frame is fixed in displaced platform such that the axes of the Z and Y frames are parallel and the origins coincident when the platform is in the null position; $\underline{S'}_i$ locates the ith laser in the fixed Y frame; $\underline{S}_i$ locates the ith laser in the displaced Z frame; $\underline{\Delta}_i$ is the vector defining the location of the ith detector with respect to the ith laser in the null position; $\underline{r}_0$ locates the CM in the Y frame; $\underline{r}_{cm}$ is the displacement of the CM with respect to the Y frame; and $\underline{\rho}$ locates the origin of the displaced platform frame with respect to the CM in the Z frame. For the STABLE configuration, position sensor locations are shown in figure 25, from which these vectors are defined as

$$\underline{r}_0 = r_1\underline{Y}_1 + r_2\underline{Y}_2 + r_3\underline{Y}_3$$

$$\underline{r}_{cm} = x_{cg}\underline{Y}_1 + y_{cg}\underline{Y}_2 + z_{cg}\underline{Y}_3$$

$$\underline{\rho} = -r_1\underline{Z}_1 - r_2\underline{Z}_2 - r_3\underline{Z}_3$$

$$\underline{S}_1 = S_1 \underline{Z}_1; \quad \underline{S}_2 = -S_2 \underline{Z}_1; \quad \underline{S}_3 = -S_3 \underline{Z}_2$$

$$\underline{S}'_1 = S_1 \underline{Y}_1; \quad \underline{S}'_2 = -S_2 \underline{Y}_1; \quad \underline{S}'_3 = -S_3 \underline{Y}_2$$

$$\underline{\Delta}_1 = \Delta_1 \underline{Y}_1; \quad \underline{\Delta}_2 = -\Delta_2 \underline{Y}_1; \quad \underline{\Delta}_3 = -\Delta_3 \underline{Y}_2 \ .$$

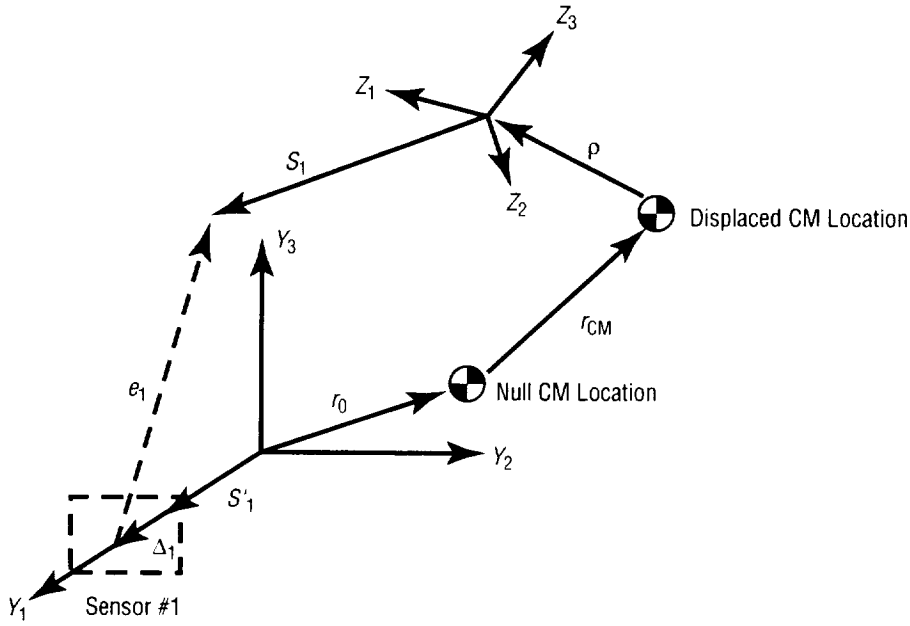

Figure 24. Definition of coordinate frames for relative position measurements.

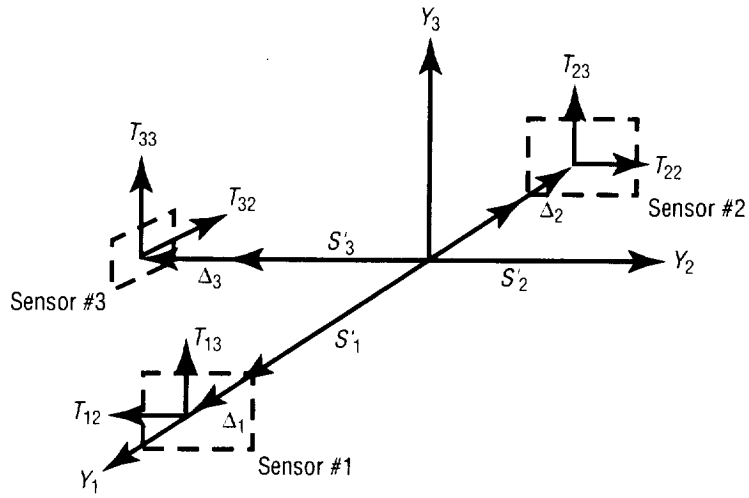

Figure 25. Position sensor detector locations.

Assuming small angles, the transformation from the Z frame to the Y frame is

$$T_{YZ} = \begin{bmatrix} 1 & -\theta_{z_{cg}} & \theta_{y_{cg}} \\ \theta_{z_{cg}} & 1 & -\theta_{x_{cg}} \\ -\theta_{y_{cg}} & \theta_{x_{cg}} & 1 \end{bmatrix} . \tag{2}$$

Realizing all vectors in the Y frame yields the error vectors

$$\underline{e}_1 = \begin{Bmatrix} e_{11} \\ e_{12} \\ e_{13} \end{Bmatrix} = \begin{Bmatrix} r_1 \\ r_2 \\ r_3 \end{Bmatrix} + \begin{Bmatrix} x_{cg} \\ y_{cg} \\ z_{cg} \end{Bmatrix} + \begin{bmatrix} 1 & -\theta_{z_{cg}} & \theta_{y_{cg}} \\ \theta_{z_{cg}} & 1 & -\theta_{x_{cg}} \\ -\theta_{y_{cg}} & \theta_{x_{cg}} & 1 \end{bmatrix} \begin{Bmatrix} -r_1 + S_1 \\ -r_2 \\ -r_3 \end{Bmatrix} + \begin{Bmatrix} -S_1 - \Delta_1 \\ 0 \\ 0 \end{Bmatrix} \tag{3}$$

$$\underline{e}_2 = \begin{Bmatrix} e_{11} \\ e_{12} \\ e_{13} \end{Bmatrix} = \begin{Bmatrix} r_1 \\ r_2 \\ r_3 \end{Bmatrix} + \begin{Bmatrix} x_{cg} \\ y_{cg} \\ z_{cg} \end{Bmatrix} + \begin{bmatrix} 1 & -\theta_{z_{cg}} & \theta_{y_{cg}} \\ \theta_{z_{cg}} & 1 & -\theta_{x_{cg}} \\ -\theta_{y_{cg}} & \theta_{x_{cg}} & 1 \end{bmatrix} \begin{Bmatrix} -r_1 - S_2 \\ -r_2 \\ -r_3 \end{Bmatrix} + \begin{Bmatrix} S_2 + \Delta_2 \\ 0 \\ 0 \end{Bmatrix} \tag{4}$$

$$\underline{e}_3 = \begin{Bmatrix} e_{11} \\ e_{12} \\ e_{13} \end{Bmatrix} = \begin{Bmatrix} r_1 \\ r_2 \\ r_3 \end{Bmatrix} + \begin{Bmatrix} x_{cg} \\ y_{cg} \\ z_{cg} \end{Bmatrix} + \begin{bmatrix} 1 & -\theta_{z_{cg}} & \theta_{y_{cg}} \\ \theta_{z_{cg}} & 1 & -\theta_{x_{cg}} \\ -\theta_{y_{cg}} & \theta_{x_{cg}} & 1 \end{bmatrix} \begin{Bmatrix} -r_1 \\ -r_2 - S_3 \\ -r_3 \end{Bmatrix} + \begin{Bmatrix} 0 \\ S_3 + \Delta_3 \\ 0 \end{Bmatrix} . \tag{5}$$

Figure 26 shows the projection of $\underline{e}_1$ onto sensor #1, for which the detector plane is the $\underline{Y}_2\,\underline{Y}_3$ plane. Note from figure 25 that the sensor frame is not aligned with the Y frame, but $\underline{T}_{11} = -\underline{Y}_1$ and $\underline{T}_{12} = -\underline{Y}_2$. The error vector originates at the center of the detector and terminates at the laser in the displaced platform frame.

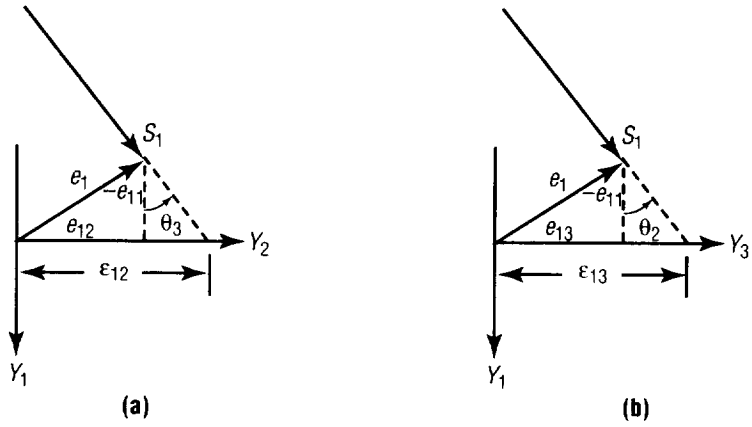

Figure 26. Error vector projection for sensor #1.

Recalling the small angle assumption, figure 26(a) indicates that the error projected in the $\underline{Y}_2$ direction on detector #1 is

$$\varepsilon^{Y}12 = e_{12} - e_{11}\theta_{z_{cg}} \quad , \tag{6}$$

and the error projected in the $\underline{Y}_3$ direction on detector #1 is

$$\varepsilon^{Y}13 = e_{13} + e_{11}\theta_{y_{cg}} \quad . \tag{7}$$

Recognizing that the actual detector error signals are in the T_1 frame, the error projection terms in equations (6) and (7) must be transformed to the T_1 frame. Substituting for the error vector components from equation (3) and neglecting higher order terms yields

$$\varepsilon^{T_1}12 = -\varepsilon^{Y}12 = -y_{cg} - r_3\theta_{x_{cg}} - (S_1 + \Delta_1 - r_1)\theta_{z_{cg}} + x_{cg}\theta_{z_{cg}} , \tag{8}$$

$$\varepsilon^{T_1}13 = \varepsilon^{Y}12 = z_{cg} - r_2\theta_{x_{cg}} - (S_1 + \Delta_1 - r_1)\theta_{y_{cg}} + x_{cg}\theta_{y_{cg}} \quad . \tag{9}$$

A similar procedure is followed for sensors #2 and #3 which results in the relative position measurements given by

$$\begin{bmatrix} \varepsilon_{12} \\ \varepsilon_{13} \\ \varepsilon_{22} \\ \varepsilon_{23} \\ \varepsilon_{32} \\ \varepsilon_{33} \end{bmatrix} = \begin{bmatrix} 0 & -1 & 0 & -r_3 & 0 & -(-r_1+S_1+\Delta_1) \\ 0 & 0 & 1 & -r_2 & -(-r_1+S_1+\Delta_1) & 0 \\ 0 & 1 & 0 & r_3 & 0 & -(r_1+S_2+\Delta_2) \\ 0 & 0 & 1 & -r_2 & (r_1+S_2+\Delta_2) & 0 \\ -1 & 0 & 0 & 0 & r_3 & -(r_2+S_3+\Delta_3) \\ 0 & 0 & 1 & -(r_2+S_3+\Delta_3) & r_1 & 0 \end{bmatrix} \begin{bmatrix} x_{cg} \\ y_{cg} \\ z_{cg} \\ \theta_{x_{cg}} \\ \theta_{y_{cg}} \\ \theta_{z_{cg}} \end{bmatrix}$$

$$+ \begin{bmatrix} x_{cg}\theta_{z_{cg}} \\ x_{cg}\theta_{y_{cg}} \\ -x_{cg}\theta_{z_{cg}} \\ x_{cg}\theta_{y_{cg}} \\ -y_{cg}\theta_{z_{cg}} \\ -y_{cg}\theta_{x_{cg}} \end{bmatrix} . \tag{10}$$

This nonlinear equation can be solved for the platform CM motion, $(x_{cg}, y_{cg}, z_{cg}, \theta_{x_{cg}}, \theta_{y_{cg}}, \theta_{z_{cg}})$ given the six sensor measurements using the following relationship:

$$\theta_{z_{cg}} = -(\varepsilon_{12}+\varepsilon_{22})/(2*(s+l)) \tag{11}$$

$$\theta_{y_{cg}} = -(\varepsilon_{13}-\varepsilon_{23})/(2*(s+l)) \tag{12}$$

$$\Gamma_1 = -\varepsilon_{33}+(\varepsilon_{13}+\varepsilon_{23})/2+\varepsilon_{32}*\theta_{y_{cg}} - r_3*\theta_{y_{cg}}{}^2 + (s_3+d+r_2)*\theta_{y_{cg}}*\theta_{z_{cg}} \tag{13}$$

$$\Gamma_2 = (\varepsilon_{22}-\varepsilon_{12})/2+r_1*\theta_{z_{cg}} + \theta_{z_{cg}}*(-\varepsilon_{32}+r_3*\theta_{y_{cg}} - (s_3+d+r_2)*\theta_{z_{cg}}) \tag{14}$$

$$\Lambda_1 = 1+\theta_{z_{cg}}{}^2 \tag{15}$$

$$\Lambda_2 = (s_3+d)*\Lambda_1 + r_3*\theta_{y_{cg}}*\theta_{z_{cg}} - \Gamma_2 \tag{16}$$

$$\Lambda_3 = r_3 * \Gamma_1 - \Gamma_2 * (s_3 + d) \tag{17}$$

$$y_{cg} = (-\Lambda_2 + \sqrt{\Lambda_2^2 - 4 * \Lambda_1 * \Lambda_3}) / (2 * \Lambda_1) \tag{18}$$

$$x_{cg} = -\varepsilon_{32} + r_3 * \theta_{y_{cg}} - (s_3 + d + r_2) * \theta_{z_{cg}} - y_{cg} * \theta_{z_{cg}} \tag{19}$$

$$\theta_{x_{cg}} = (\Gamma_1 + \theta_{y_{cg}} * \theta_{z_{cg}} * y_{cg}) / (s_3 + d + y_{cg}) \tag{20}$$

$$z_{cg} = (\varepsilon_{13} + \varepsilon_{23}) / 2 + r_2 * \theta_{x_{cg}} - r_1 * \theta_{y_{cg}} - \theta_{x_{cg}} * \theta_{y_{cg}} \ , \tag{21}$$

where $S_1 = S_2 = s$; $S_3 = s_3$; and $\Delta_1 = \Delta_2 = \Delta_3 = d$.

A.2 Relative Displacements at the Actuator Gap

The displacements at the actuator gap may now be determined from the displacements of the platform CM computed using equations (11)–(21). Figure 27 indicates the same coordinate frames and vectors locating the CM as figure 24 and also introduces the vector defining the location of the center of the gap associated with actuator #*i* (*i*=1,2,3), designated by R_i in the *Y* frame and by R_i' in the *Z* frame. From figure 27, the relative displacement measured at the gap of actuator #*i* is

$$\underline{\delta}_i = -\underline{R}_i + \underline{r}_0 + \underline{r}_{cm} + \underline{\rho} + \underline{R}'_i \ . \tag{22}$$

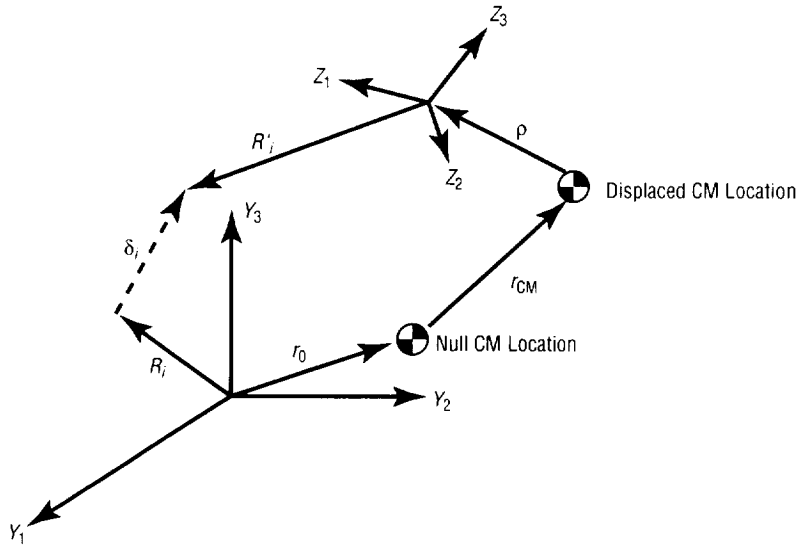

Figure 27. Relative displacement vector at actuator gap.

Note that the location of the CM vector is now defined with respect to the Z frame as

$$\underline{r}_{cm} = x_{cg}\underline{Z}_1 + y_{cg}\underline{Z}_2 + z_{cg}\underline{Z}_3 \quad , \tag{23}$$

and

$$\underline{R}_i = R_{i1}\underline{Y}_1 + R_{i2}\underline{Y}_2 + R_{i3}\underline{Y}_3 \tag{24}$$

$$\underline{R}'_i = R_{i1}\underline{Z}_1 + R_{i2}\underline{Z}_2 + R_{i3}Z_3 \quad . \tag{25}$$

The actuator local coordinate frames are defined in figure 28 with the transformation matrices $T_{ZY} = T_{YZ}^T$ (from equation (2)), $T_{S_1Z} = I$, and $T_{S_3Z} = T_{S_2Z}^T$ where

$$T_{S_2Z} = \begin{bmatrix} -a & a & 0 \\ -a & -a & 0 \\ 0 & 0 & 1 \end{bmatrix} , \tag{26}$$

and $a = \sqrt{2}/2$.

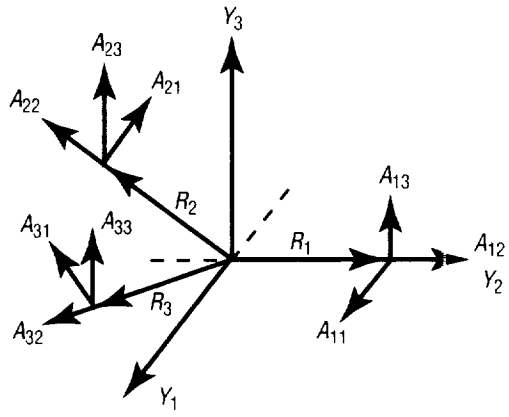

Figure 28. Actuator coordinate frames.

Equation (22) may now be evaluated for the relative displacement at the gap of actuator #*i* in the *Z* coordinate frame:

$$\underline{\delta}_i = \begin{bmatrix} 1 & \theta_{z_{cg}} & -\theta_{y_{cg}} \\ -\theta_{z_{cg}} & 1 & \theta_{x_{cg}} \\ \theta_{y_{cg}} & -\theta_{x_{cg}} & 1 \end{bmatrix} \begin{Bmatrix} -R_{i1} + r_1 \\ -R_{i2} + r_2 \\ -R_{i3} + r_3 \end{Bmatrix} + \begin{Bmatrix} x_{cg} - r_1 + R_{i1} \\ y_{cg} - r_2 + R_{i2} \\ z_{cg} - r_3 + R_{i3} \end{Bmatrix} . \tag{27}$$

After simplifying,

$$\underline{\delta}_i = \begin{Bmatrix} x_{cg} + (R_{i3} - r_3)\theta_{y_{cg}} - (R_{i2} - r_2)\theta_{z_{cg}} \\ y_{cg} - (R_{i3} - r_3)\theta_{x_{cg}} + (R_{i1} - r_1)\theta_{z_{cg}} \\ z_{cg} + (R_{i2} - r_2)\theta_{x_{cg}} - (R_{i1} - r_1)\theta_{y_{cg}} \end{Bmatrix} .$$

The gap displacements must be expressed in the appropriate actuator frame using the transformation matrices defined in equation (26) and the immediately preceding text. In the actuator frames, $\underline{\delta}_i^{S_i} = T_{S_i Z}\,\underline{\delta}_i^{Z}$, which results in

$$\begin{bmatrix} \delta_{11} \\ \delta_{13} \\ \delta_{21} \\ \delta_{23} \\ \delta_{31} \\ \delta_{33} \end{bmatrix} = \begin{bmatrix} 0 & 0 & 0 & 0 & (R_{13} - r_3) & -(R_{12} - r_2) \\ 0 & 0 & 1 & (R_{12} - r_2) & -(R_{11} - r_1) & 0 \\ -a & a & 0 & -a(R_{23} - r_3) & -a(R_{23} - r_3) & a(R_{21} - r_1 + R_{22} - r_2) \\ 0 & 0 & 1 & (R_{22} - r_2) & -a(R_{21} - r_1) & 0 \\ -a & -a & 0 & a(R_{33} - r_3) & -a(R_{33} - r_3) & a(R_{32} - r_2 - R_{31} + r_1) \\ 0 & 0 & 1 & (R_{32} - r_2) & -(R_{31} - r_1) & 0 \end{bmatrix} \begin{bmatrix} x_{cg} \\ y_{cg} \\ z_{cg} \\ \theta_{x_{cg}} \\ \theta_{y_{cg}} \\ \theta_{z_{cg}} \end{bmatrix} . \tag{28}$$

REFERENCES

1. Edberg, D.; Boucher, R.; Schenck, D.; Nurre, G.; Whorton, M.; Kim, Y.; and Alhorn, D.: "Results of the STABLE Microgravity Vibration Isolation Flight Experiment," AAS 96–071, Presented to the 19th Annual AAD Guidance and Control Conference, Breckenridge, CO, February 7–11, 1996.

2. "User's Manual for TREETOPS, A Control System Simulation for Structures With a Tree Topology," NASA Contract NAS–36287, Marshall Space Flight Center, AL. April 1990.

3. Whorton, M.S.: "Documentation of the STABLE TREETOPS Parameter File and Control Law Subroutines," NASA Internal Memorandum ED11–12–98-231.

REPORT DOCUMENTATION PAGE

Form Approved
OMB No. 0704-0188

1. AGENCY USE ONLY *(Leave Blank)*	2. REPORT DATE	3. REPORT TYPE AND DATES COVERED
	January 1999	Technical Memorandum

4. TITLE AND SUBTITLE

A TREETOPS Simulation of the STABLE Microgravity Vibration Isolation System

5. FUNDING NUMBERS

6. AUTHORS

G.S. Nurre, Y.K. Kim,* and M.S. Whorton

7. PERFORMING ORGANIZATION NAMES(S) AND ADDRESS(ES)

George C. Marshall Space Flight Center
Marshall Space Flight Center, Alabama 35812

8. PERFORMING ORGANIZATION REPORT NUMBER

M–906

9. SPONSORING/MONITORING AGENCY NAME(S) AND ADDRESS(ES)

National Aeronautics and Space Administration
Washington, DC 20346–0001

10. SPONSORING/MONITORING AGENCY REPORT NUMBER

NASA/TM—1999–209009

11. SUPPLEMENTARY NOTES

Prepared by the Structures and Dynamics Laboratory, Science and Engineering Directorate
*University of Alabama in Huntsville

12a. DISTRIBUTION/AVAILABILITY STATEMENT

Unclassified–Unlimited
Subject Category 18
Nonstandard Distribution

12b. DISTRIBUTION CODE

13. ABSTRACT *(Maximum 200 words)*

As a research facility for microgravity science, the *International Space Station (ISS)* will be used for numerous experiments which require a quiescent acceleration environment across a broad spectrum of frequencies. For many microgravity science experiments, the ambient acceleration environment on *ISS* will significantly exceed desirable levels. The ubiquity of acceleration disturbance sources and the difficulty in characterization of these sources precludes source isolation, requiring vibration isolation to attenuate the disturbances to an acceptable level at the experiment. To provide a more quiescent acceleration environment, a vibration isolation system named STABLE (Suppression of Transient Accelerations By LEvitation) was developed. STABLE was the first successful flight test of an active isolation device for microgravity science payloads and was flown on STS-73/USML-2 in October 1995. This report documents the development of the high fidelity, nonlinear, multibody simulation developed using TREETOPS which was used to design the control laws and define the expected performance of the STABLE isolation system.

14. SUBJECT TERMS

microgravity, vibration isolation, simulation, STABLE

15. NUMBER OF PAGES

56

16. PRICE CODE

A04

17. SECURITY CLASSIFICATION OF REPORT	18. SECURITY CLASSIFICATION OF THIS PAGE	19. SECURITY CLASSIFICATION OF ABSTRACT	20. LIMITATION OF ABSTRACT
Unclassified	Unclassified	Unclassified	Unlimited

APPROVAL

A TREETOPS SIMULATION OF THE STABLE MICROGRAVITY VIBRATION ISOLATION SYSTEM

G.S. Nurre, Y.K. Kim, and M.S. Whorton

The information in this report has been reviewed for technical content. Review of any information concerning Department of Defense or nuclear energy activities or programs has been made by the MSFC Security Classification Officer. This report, in its entirety, has been determined to be unclassified.

W.R. HUMPHRIES
DIRECTOR, STRUCTURES AND DYNAMICS LABORATORY